Research Article

Xiaoming Wang, Usama Ghafoor, Muhammad Abbas*, Farah Aini Abdullah*, and Yasser Salah Hamed

Effectual quintic B-spline functions for solving the time fractional coupled Boussinesq–Burgers equation arising in shallow water waves

https://doi.org/10.1515/phys-2025-0191
received March 06, 2025; accepted June 10, 2025

Abstract: This article investigates fluid flow in a dynamic system using the coupled Boussinesq–Burgers equation to precisely narrate the propagation of shallow water waves. This work proposes a novel approach to using the quintic B-spline technique to obtain an approximate solution to the nonlinear fractional coupled Boussinesq–Burgers equation. For discretizing time, the Caputo fractional derivative is used to handle the fractional derivative effectively, while the quintic B-spline function is used to interpolate the spatial derivative. We provide two numerical examples to show the level of accuracy and practicality of the current scheme in solving the fractional coupled Boussinesq–Burgers problem and see how observe the effect of the fractional-order on wave propagation. In addition, we conduct a stability analyzis and numerically determine the order of convergence. We compute the error norms to assess the accuracy of the proposed method.

Keywords: Boussinesq–Burgers equation, quintic B-spline functions, Caputo time fractional derivative, finite difference technique, stability

*** Corresponding author: Muhammad Abbas,** Department of Mathematics, University of Sargodha, Sargodha 40100, Pakistan, e-mail: muhammad.abbas@uos.edu.pk
*** Corresponding author: Farah Aini Abdullah,** School of Mathematical Sciences, Universiti Sains Malaysia, 11800 USM Pulau Pinang, Malaysia, e-mail: farahaini@usm.my
Xiaoming Wang: School of Mathematics and Computer Science, Shangrao Normal University, Shangrao 334001, China
Usama Ghafoor: Department of Mathematics, University of Sargodha, Sargodha 40100, Pakistan
Yasser Salah Hamed: Department of Mathematics and Statistics, College of Science, Taif University, P. O. Box 11099, Taif 21944, Saudi Arabia

1 Introduction

During the past few decades, there has been an increased amount of research on the use of fractional derivatives instead of integer derivatives and on the implementation of fractional integrals, fractional differential equations (FDEs), and fractional partial differential equations (FPDEs) in solving a series of problems arising in the pure and applied sciences [1–4]. The generalization of classical differential equations of integer order (IO) give rise to FDEs. Many complicated nonlinear phenomena that arise in the fields of heat transfer, wave propagation, and other subjects have been extensively described using fractional calculus, as is well known. Therefore, to describe physics, engineering, and other scientific subjects, FPDEs are crucial [5–8]. The fact that the response of the fractional-order system eventually converges to the response of the IO system has drawn a lot of attention to FDEs [9]. Their nonlocal characteristic is the primary benefit of employing fractional-order FDEs in various mathematical modelling. Many works have been accomplished to obtain the necessary mathematical methods for dealing with fractional problems. The goal of our investigation is to look for approximate results of time-fractional coupled Boussinesq–Burgers equation (TFCBBE) that is a nonlinear system. We investigate a time-fractional model of the coupled Boussinesq–Burgers equation (CBBE), which arises from the study of fluid flow dynamics, specifically the transmission of waves in shallow water. This model describes a wide range of physical phenomena in disciplines such as chemical physics, solid-state physics, fluid mechanics, and plasma waves. Exploring its solutions and properties is essential to understanding these phenomena, as solutions not only address specific problems but also offer deeper insights into the underlying physical processes. For instance, nonlinear wave behaviours in fluid dynamics, plasma, and optical fibers are often represented by characteristic bell-shaped and kink-shaped solutions.

As noted in the literature, Zhang *et al.* [10] proposed a (2 + 1)-dimensional Boussinesq–Burgers soliton (BBS)

equation and its connection with the BBS hierarchy. They proved that quasi-periodic solutions of the (2 + 1)-dimensional BBE are derived by resorting to the Riemann θ functions. Zhang *et al.* [11] investigated the exact solutions of the generalized Boussinesq equation and the BBE using the modified mapping method. Rady *et al.* [12] showed that the periodic wave solutions for BBE are obtained by using the Jacobi elliptic function method and presented the properties of some periodic and multiple soliton solutions. Chen and Li [13] presented a new Darboux transformation with multiple parameters for BBE using Darboux transformation and found new soliton solutions of the BBS. Gupta and Ray [14] proposed the comparison between the homotopy perturbation method (HPM) and the optimal homotopy asymptotic method (OHAM) using approximate solution of nonlinear BBE and concluded that optimal homotopy asymptotic method is accurate with a smaller number of iterations compared to the HPM, while the OHAM introduces a simple way to control convergence region.

Wang *et al.* [15] investigated the approximate solution of fractal CBBE using the semi-inverse method and established the fractal variational formulation of fractal CBBE. Kumar *et al.* [16] represented the approximate solution of CBBE using residual power series method and compared their results with the analytical solutions as well as the solutions shown on different graphical representations. They also obtained the solution by the modified homotopy analyzis transform method. Khater and Kumar [17] constructed exact solutions for the fractional CBBE using fractional complex transform and the modified Riemann Liouville derivative sense. Shi *et al.* [18] investigated into a few of the time-fractional CBBE's invariant characteristics. First, using the discovered symmetries, the fractional CBBE is converted into nonlinear time FDEs. Second, they used a power series expansion method to solve the reduced system of fractional ordinary differential equations. Third, the new conservation theorem is used to derive the conservation rules of the fractional CBBE. Ravi *et al.* [19] analyzed the exact solutions of CBBE using analytically as well use the Exp-function method. They also shown their result graphically. Ali *et al.* [20] investigated the analytical solution of CBBE through the sine-Gordon expansion method and results shown on 2D and 3D plotting. Heydari and Avazzadeh [21] introduced the approximate solution of CBBE by using the concept of the Caputo form. Zarin *et al.* [22] analyzed the fractional-order susceptible infected recovered again susceptible model using Caputo derivatives and solved numerically using the Haar collocation-Broyden method. Jitsinchayakul *et al.* [23] proposed the fractional-order COVID-19 epidemic model using the Atangana–Baleanu–Caputo fractional operator and analyzed the results. Chu *et al.* [24] presented a fractional-order SARS-CoV-2 transmission model using the Atangana–Baleanu derivative and solved numerically using Newton polynomial-based iterative scheme. Zarin *et al.* [25] investigated reaction–diffusion COVID-19 model using the next-generation method and solved numerically using finite difference and a one-step explicit meshless scheme. Zhang and Whang [26] presented the numerical solution of coupled Burgers equations using a space-time semi-analytical meshless scheme and radial and non-radial basis functions. Wang *et al.* [27] investigated the approximate solution of the Burgers equation using the multistage homotopy asymptotic method and compared their result for a large time span.

Iqbal *et al.* [28] investigated the theoretical foundation of the nonlinear Schrödinger equation is connected with real-world ocean engineering applications in this article, which offers solutions that demonstrate several wave forms, including solitons and periodic waves, utilizing three different approaches. Deepening our grasp of wave dynamics and improving underwater engineering and design are the goals of these efforts. Rehman *et al.* [29] used two new mathematical techniques to analyze the (3 + 1)-dimensional extended quantum Zakharov–Kuznetsov equation in plasma and obtain a variety of soliton solutions. The results provide useful tools for investigating nonlinear evolution equations and provide fresh perspectives on the dynamics of the model, as demonstrated by 2D, 3D, and contour plots. Iqbal *et al.* [30] utilized novel techniques to acquire different optical soliton solutions of the Sasa–Satsuma equation, which simulates the propagation of femtosecond pulses in optical fibres. These results improve our knowledge of optical phenomena and present new methods for studying nonlinear optical systems. Zhu *et al.* [31] investigated special solitary wave solutions of the Heisenberg ferromagnetic spin chain equation and uncover its function in nonlinear wave dynamics. They show how these solutions improve knowledge of solitons in mathematical physics and its applications in domains such as fluid dynamics and fibre optics using straightforward but powerful analytical methods. Kai and Yin [32] presented a broad multi-wave solution framework by using the Cole–Hopf transformation to reveal the linear structure of the Sharma–Tasso–Olver–Burgers equation. Notably, it uses bifurcation techniques to expose the paths of dark-bright and kink–kink soliton molecules, as well as their fusion and fission processes. He and Kai [33] analyzed Kudryashov's equation with third-order dispersion, periodic and soliton solutions, and exploring modulation instability and chaotic behaviour under many perturbations. The findings provide valuable insights into the equation's wave dynamics and potential applications in complex phenomena. Xie *et al.* [34] proposed freedom asymmetric Duffing system of degree two with fractional damping and stability analysis using approximate methods. The study highlights the impact of fractional damping on controlling rotor vibrations and practical

applications in vibration management. Kumar *et al.* [35] presented the exact solitary wave solutions of the strain wave equation using the generalized exponential rational function method and proved the effectiveness of the method with clear physical interpretations. Kumar *et al.* [36] investigated the (1 + 1)-dimensional longitudinal wave equation to derive a novel solitary wave using the unified method and the unified Riccati equation expansion method. Kumar *et al.* [37] analyzed the Wazwaz–Benjamin–Bona–Mahony equation using Adomian, Lie isomorphism, and unified Riccati equation expansion methods to obtain exact soliton solutions. Hussain *et al.* [38] solved the nonlinear Benjamin Bona Mahony Burgers equation to obtain the soliton solutions using extended $\exp(-\Phi(\chi))$ expansion and Kudryashov methods and analyzis of the fluid dynamics. Hussain *et al.* [39] investigated the nonlinear Sharma Tasso Olver Burgers equation using the extended $(\frac{\dot{G}}{G^2})$ expansion method to obtain soliton solutions and analyzis the stability, and sensitivity.

The present study employs the quintic B-spline (QBS) method in conjunction with the Caputo derivative for the numerical solution of the TFCBBE. The $L1$ formula is applied for handling the non-IO derivative, whereas the discretization of the space derivative is carried out with the help of B-spline functions. The benefits of utilizing the spline collocation technique in comparison to the currently available methods lie in its ability to effectively provide a piecewise continuous, closed-form solution. In addition, it offers a more straightforward approach and can be applied to a diverse set of problems related to partial and FPDEs. The superiority of this approach compared to alternative techniques lies in the fact that upon obtaining the solution, the requisite data for interpolation at various points within the range becomes accessible. The primary advantage of this technique is its capability to closely approximate the analytical curve up to a specified level of continuity. Consequently, the spline methodology offers more precise outcomes when estimating values at any given location in the field, in contrast to its predecessors.

Several researchers have used numerical methods to solve FPDEs. The presented method is innovative in that it uses a Crank–Nicolson scheme to discretize the fractional derivative. This method is chosen for its suitability in capturing complex nonlinear wave behaviours, such as bell-shaped and kink-shaped waves in fluid dynamics and optics. Spatial derivatives for TECBBE are discretized using QBS functions. The proposed scheme is novel, and as far as we are aware, the fractional derivative in the Caputo sense has never been employed for the numerical solution of TFCBBE using QBS functions before. The article commences by presenting the TFCBBE as a means for determining numerical solutions to the TFCBBE with the help of the Crank–Nicolson approach. This innovative technique depends on the θ-weighted scheme and the Caputo operator. Initially, we constructed the QBS function across the entire domain and employed the Caputo time fractional derivative for temporal discretization. In addition, a numerical method is introduced that utilizes a θ-weighted scheme and quasi-linearization. Subsequently, a stability analyzis is conducted. Finally, two numerical test problems are provided to demonstrate the suggested technique, together with their corresponding graphical representation. Concluding remarks are provided at the conclusion of the article.

In this work, the QBS functions are used to solve the TFCBBE numerically. They are piecewise polynomial functions, which are smooth and offer flexibility in approximating solutions. The QBS, which are fifth-degree polynomials, offer C^4 continuity, ensuring smooth transitions at each joint between piecewise segments, which is valuable for accurately approximating solutions to differential equations. The CBBE model has been previously solved using the QBS approach combined with the Crank–Nicolson formulation. Moreover, the time-fractional version of this model has been addressed using the time-spectrum function method, the power series expansion method and the homotopy perturbation method. However, no research has been conducted for solving the TFCBBE model using the QBS approach alongside the Crank–Nicolson scheme. This gap highlights the unique contribution of this study, offering a novel approach for solving the time-fractional version of the model. The novelty of this work lies in the numerical solution of the fractional CBBE by employing the Caputo fractional derivative for time discretization and QBS functions for spatial discretization. This innovative approach allows for accurate and effective solutions at each node, offering a unique and effective method for addressing the fractional CBBE. This combination improves accuracy and stability by balancing the time step's implicit and explicit contributions. Compared to current approaches, this methodology has the advantage of improved numerical solution smoothness and precision. This particular time-fractional equation has never before been solved using such a combination, illustrating the method's superiority in providing an accurate, piecewise cubic, and smooth solution for complex fractional-order equations.

The article is organized as follows: In Section 2, the TFCBBE model is presented along with the necessary initial and boundary conditions (BCs). The preliminaries are described, consisting of two subsections. Caputo fractional derivative is presented in subsection 3.1, and subsection 3.2 provides an overview of the QBS functions at various points. Section 4 discusses the process of discretizing the fractional derivative, whereas Section 5 outlines the steps involved in the suggested numerical technique. Section 6 establishes the starting condition for the approximate solution. Section 7 provides the algorithm of our numerical technique. Sections 8 and 9 examine the stability and convergence analyzis of the

proposed methodology. Section 10 presents the numerical test problems. Section 11 outlines the study's conclusion.

2 Model

The TFCBBE, with real-valued functions $U(x,t)$ and $V(x,t)$, takes the following form (Table 1):

$$\begin{cases} U_t^{\lambda}(x,t) + a_1 V_x(x,t) + b_1 U(x,t) U_x(x,t) = Q_1(x,t), \\ V_t^{\lambda}(x,t) + a_2 U_{xxx}(x,t) + b_2 (U(x,t)V(x,t))_x \\ \quad = Q_2(x,t), \\ a \le x \le b, \quad 0 \le t \le T \end{cases} \tag{2.1}$$

with initial conditions (ICs)

$$\begin{cases} U(x,0) = f(x), \\ V(x,0) = g(x), \end{cases} \tag{2.2}$$

and BCs

$$\begin{cases} U(a,t) = f_1(a,t), & V(a,t) = g_1(a,t), \\ U(b,t) = f_2(b,t), & V(b,t) = g_2(b,t), \\ U_x(a,t) = f_3(a,t), & V_x(a,t) = g_3(a,t), \\ U_x(b,t) = f_4(b,t), & V_x(b,t) = g_4(b,t). \end{cases}$$

3 Preliminaries

3.1 Caputo fractional derivative

Various strategies exist for handling fractional derivative, while the Caputo $L1$ formula is more preferable fractional derivative to studied real-world physical model. Because it employ memory effects and non-local behaviour, the Caputo fractional derivative is a great tool for simulation and may be utilized for a variety of real-world systems and phenomena. It possess remarkable physical interpretability, effectively capturing memory effects and non-local characteristics in systems, finding them ideal for simulating a variety of phenomena in a number of fields. Caputo's fractional derivative is applied to discretize the temporal derivative, which is given as follows:

$${}^{C}U_t^{\lambda}(x,t) = \begin{cases} \dfrac{1}{\Gamma(1-\lambda)} \displaystyle\int_0^t U_{\chi}(x,\chi)(t-\chi)^{-\lambda} \mathrm{d}\chi, & 0 < \lambda < 1, \\ U_t(x,t), & \lambda = 1. \end{cases} \tag{3.1}$$

Table 1: Variable descriptions

Parameter	Description
$U(x,t)$	Horizontal velocity field
$V(x,t)$	Height of the water surface above a horizontal level at the bottom
x	Normalized space variable
t	Normalized time variable
$Q_1(x,t), Q_2(x,t)$	Source terms
a_1, a_2, b_1, b_2	Constants
$f(x), g(x)$	Known function
$f_1(a,t), f_2(a,t), f_3(a,t), f_4(a,t)$	Known functions
$g_1(a,t), g_2(a,t), g_3(a,t), g_4(a,t)$	Known functions
λ	Fractional order which $\in(0,1)$
Γ	Euler's Gamma function
h	Step size for space
τ	Step size for time

3.2 QBS

We uniformly divide the space interval $[x_{\min}, x_{\max}]$ by $N+1$ knots such that the grid distribution is $a = x_{\min} < \cdots < x_{\max} = b$, *i.e.*, $x_j = x_0 + jh$, $j = 0(1)N$, uniform mesh size is $h = \frac{x_{\max} - x_{\min}}{N}$. The jth basis spline function of order q, degree $q-1$, is given by [40]:

For $q = 0$,

$$B_{0,j}(x) = \begin{cases} 1, & \text{if } x \in [x_j, x_{j+1}] \\ 0, & \text{otherwise}. \end{cases} \tag{3.2}$$

For $q > 0$,

$$\begin{aligned} B_{q,j}(x) = {} & \frac{x - x_j}{x_{j+q} - x_j} B_{q-1,j}(x) \\ & + \left(1 - \frac{x - x_{j+1}}{x_{j+1+q} - x_{j+1}}\right) B_{q-1,j+1}(x), \\ & x \in [x_j, x_{j+1+q}]. \end{aligned} \tag{3.3}$$

We extend the interval $[x_{\min}, x_{\max}]$ to interval $[x_{\min} - 5h, x_{\max} + 5h]$ with uniform mesh and the relationships listed below define the piecewise QBS basis functions $(B_j(x))$ [41]:

$$B_{5,j}(x) = \frac{1}{6h^3} \begin{cases} c_1, & \text{if } x \in [x_{j-3}, x_{j-2}], \\ c_1 - 6c_2, & \text{if } x \in [x_{j-2}, x_{j-1}], \\ c_1 + 15c_3 - 6c_2, & \text{if } x \in [x_{j-1}, x_j], \\ c_4 - 15c_6 + 6c_5, & \text{if } x \in [x_j, x_{j+1}], \\ c_4 + 6c_5, & \text{if } x \in [x_{j+1}, x_{j+2}], \\ c_4, & \text{if } x \in [x_{j+2}, x_{j+3}], \\ 0, & \text{otherwise}, \end{cases} \tag{3.4}$$

where $c_1 = (x - x_{j-3})^5$, $c_2 = (x - x_{j-2})^5$, $c_3 = (x - x_{j-1})^5$, $c_4 = -(x - x_{j+3})^5$, $c_5 = (x - x_{j+2})^5$, $c_6 = (x - x_{j+1})^5$. It is possible to calculate the values of $B_j(x)$ and its associated derivatives at the knot points by using piecewise QBS basis functions. It is easy to arrange these values into an equation. Now, we suppose that U and V are the approximating solutions over the subinterval $[a, b]$ using the piecewise QBS basis functions $B_j(x)$, such that:

$$\begin{cases} U(x,t) = \sum_{j=-2}^{N+2} \alpha_j^p(t) B_j(x), \\ V(x,t) = \sum_{j=-2}^{N+2} \beta_j^p(t) B_j(x). \end{cases} \tag{3.5}$$

The time-dependent parameters $\alpha_j^p(t)$ and $\beta_j^p(t)$ can be computed at each knot for the numerical solution to the exact solutions and N denotes the number of nodal points. The approximate values of $U(x,t)$ and $V(x,t)$, along with their necessary derivatives at the nodal points involving five unknowns, are calculated using an approximate function and piecewise QBS basis functions, which is defined as follows:

$$\begin{cases} (U)_j^p = \alpha_{j-2}^p + 26\alpha_{j-1}^p + 66\alpha_j^p + 26\alpha_{j+1}^p + \alpha_{j+2}^p, \\ (U_x)_j^p = -d_1\alpha_{j-2}^p - 10d_1\alpha_{j-1}^p + 10d_1\alpha_{j+1}^p + d_1\alpha_{j+2}^p, \\ (U_{xx})_j^p = d_2\alpha_{j-2}^p + 2d_2\alpha_{j-1}^p - 6d_2\alpha_j^p + 2d_2\alpha_{j+1}^p \\ \qquad + d_2\alpha_{j+2}^p, \\ (U_{xxx})_j^p = -d_3\alpha_{j-2}^k + 2d_3\alpha_{j-1}^p - 2d_3\alpha_{j+1}^p + d_3\alpha_{j+2}^p. \\ (V)_j^p = \beta_{j-2}^p + 26\beta_{j-1}^p + 66\beta_j^p + 26\beta_{j+1}^p + \beta_{j+2}^p, \\ (V_x)_j^p = -d_1\beta_{j-2}^p - 10d_1\beta_{j-1}^p + 10d_1\beta_{j+1}^p + d_1\beta_{j+2}^p, \\ (V_{xx})_j^p = d_2\beta_{j-2}^p + 2d_2\beta_{j-1}^p - 6d_2\beta_j^p + 2d_2\beta_{j+1}^p \\ \qquad + d_2\beta_{j+2}^p, \\ (V_{xxx})_j^p = -d_3\beta_{j-2}^k + 2d_3\beta_{j-1}^p - 2d_3\beta_{j+1}^p + d_3\beta_{j+2}^p, \end{cases} \tag{3.6}$$

where, $d_1 = \frac{5}{h}$, $d_2 = \frac{20}{h^2}$, $d_3 = \frac{60}{h^3}$.

4 Illustration of the scheme

The technique of forward finite difference is utilized for the discretization of the Caputo fractional derivative. Consider step size is $\tau = \frac{T}{M}$ and $t_p = p\tau$, where $p = 0, 1, \ldots, M$. At point t_p, Caputo's $L1$ formula [42] can be defined as follows:

$$\begin{aligned} {}^{C}U_t^{\lambda}(x, t_{p+1}) &= \frac{1}{\Gamma(1-\lambda)} \int_0^t U_\chi(x,\chi) \frac{d\chi}{(t_{p+1}-\chi)^\lambda} \\ &= \frac{1}{\Gamma(1-\lambda)} \sum_{s=0}^{p} \int_{t_s}^{t_{s+1}} U_\chi(x,\chi) \frac{d\chi}{(t_{p+1}-\chi)^\lambda} \\ &= \frac{1}{\Gamma(2-\lambda)} \sum_{s=0}^{p} A_s \frac{U(x, t_{1-s+p}) - U(x, t_{p-s})}{\tau^\lambda} + B_\tau^{p+1}, \end{aligned} \tag{4.1}$$

where $A_s = (s+1)^{-\lambda+1} - s^{-\lambda+1}$ and B_τ^{p+1} is bounded truncation error, *i.e.* $|B_\tau^{p+1}| \le \Theta\tau^{2-\lambda}$ [43], where Θ is the constant which depends upon U.

The coefficients A_s preserve the following properties [44]:

$$\begin{cases} A_0 = 1, \\ A_0 > A_1 > A_2 > \ldots > A_s, A_s \to 0 \quad \text{as } s \to \infty, \\ A_s > 0 \quad \text{for } s = 0, 1, \ldots p, \\ \sum_{s=0}^{p} (A_s - A_{s+1}) + A_{p+1} = (1 - A_1) + \sum_{s=1}^{p-1} (A_s - A_{s+1}) + A_p = 1. \end{cases}$$

5 Numerical technique

The θ-weighted scheme is used to find the approximate solution of the system (2.1) at t_{p+1}^{th} time level, which can be written as follows [45]:

$$\begin{cases} ({}^{C}U_t^{\lambda})_j^p - \theta g_j^{p+1} = (1-\theta) g_j^p, \\ ({}^{C}V_t^{\lambda})_j^p - \theta h_j^{p+1} = (1-\theta) h_j^p, \end{cases} \tag{5.1}$$

where

$$\begin{cases} g_j^p = -a_1 (V_x)_j^p - b_1 (UU_x)_j^p, \\ h_j^p = -a_2 (U_{xxx})_j^p - b_2 ((UV)_x)_j^p. \end{cases}$$

Setting the value of θ yields three schemes. First, when θ is set to 0, the scheme mentioned earlier turns into an explicit scheme. The second is that when $\theta = 1$, θ-weighted scheme transforms into an implicit scheme. Finally, when $\theta = 1/2$ is taken, the scheme transforms to the Crank–Nicolson scheme because it is an unconditionally stable scheme that provides reasonable accuracy. By employing Eqs. (5.1) and (2.1), we obtained:

$$\begin{aligned} &\sum_{s=0}^{p} A_s \frac{(U_j^{1-s+p} - U_j^{p-s})}{\tau^\lambda \Gamma(2-\lambda)} + \theta(a_1 (V_x)_j^{p+1} + b_1 (UU_x)_j^{p+1}) \\ &\quad = (\theta - 1)(a_1 (V_x)_j^p + b_1 (UU_x)_j^p) + Q_1, \end{aligned} \tag{5.2}$$

$$\begin{aligned} &\sum_{s=0}^{p} A_s \frac{(V_j^{1-s+p} - V_j^{p-s})}{\tau^\lambda \Gamma(2-\lambda)} + \theta(a_2 (U_{xxx})_j^{p+1} + b_2 ((UV)_x)_j^{p+1}) \\ &\quad = (\theta - 1)(a_2 (U_{xxx})_j^p + b_2 ((UV)_x)_j^p) + Q_2. \end{aligned} \tag{5.3}$$

Eqs. (5.2) and (5.3) contain non-linear terms that we aim to linearize at the $(p+1)$th stage. By simplifying complex non-linear terms, this linearization technique [46] facilitates iterative equation solving, which is defined as follows:

$$\begin{cases}(UU_x)_j^{p+1} = U_j^p(U_x)_j^{p+1} - (UU_x)_j^p + U_j^{p+1}(U_x)_j^p.\\ ((UV)_x)_j^{p+1} = (U_xV)^{p+1} + (UV_x)^{p+1}.\end{cases}$$

Using above relation, Eqs. (5.2) and (5.3) become:

$$\begin{aligned}&C\sum_{s=0}^{p}A_s(U_j^{1-s+p} - U_j^{p-s}) + a_1\theta(V_x)_j^{p+1}\\ &\quad + b_1\theta(U_j^p(U_x)_j^{p+1} + U_j^{p+1}(U_x)_j^p - (UU_x)_j^p)\\ &\quad = (\theta-1)(a_1(V_x)_j^p + b_1(UU_x)_j^p) + Q_1,\end{aligned} \tag{5.4}$$

$$\begin{aligned}&C\sum_{s=0}^{p}A_s(V_j^{1-s+p} - V_j^{p-s})\\ &\quad + a_2\theta(U_{xxx})_j^{p+1} + b_2\theta((U_xV)^{p+1} + (UV_x)^{p+1})\\ &\quad = (\theta-1)(a_2(U_{xxx})_j^p + b_2(UV_x)_j^p) + Q_2,\end{aligned} \tag{5.5}$$

where $C = \frac{1}{\tau^\lambda\Gamma(2-\lambda)}$. After simplification, Eqs. (5.4) and (5.5) are yield into Eqs. (5.6) and (5.7):

$$\begin{aligned}&CA_0U_j^{p+1} + b_1\theta(U_j^p(U_x)_j^{p+1} + U_j^{p+1}(U_x)_j^p) + a_1\theta(V_x)_j^{p+1}\\ &\quad = CA_0U_j^p - C\sum_{s=1}^{p}A_s(U_j^{p-s+1} - U_j^{p-s}) + (\theta-1)a_1(V_x)_j^p\\ &\quad + (2\theta-1)b_1(UU_x)_j^p + (Q_1)_j^{p+1},\end{aligned} \tag{5.6}$$

$$\begin{aligned}&CA_0V_j^{p+1} + b_2\theta((U_x)_j^pV_j^{p+1} + U_j^p(V_x)_j^{p+1})\\ &\quad + a_2\theta(U_{xxx})_j^{p+1} + b_2\theta(V_j^p(U_x)_j^{p+1} + (V_x)_j^pU_j^{p+1})\\ &\quad = CA_0V_j^p - C\sum_{s=1}^{p}A_s(V_j^{p-s+1} - V_j^{p-s}) + a_2(\theta-1)(U_{xxx})_j^p\\ &\quad + (2\theta-1)b_2((U_xV)_j^p + (UV_x)_j^p) + (Q_2)_j^{p+1}.\end{aligned} \tag{5.7}$$

By putting the values of QBS basis function in Eqs. (5.6) and (5.7), then we obtained Eqs. (5.8) and (5.9):

$$\begin{aligned}&D_1\alpha_{j-2}^{p+1} + D_2\alpha_{j-1}^{p+1} + D_3\alpha_j^{p+1} + D_4\alpha_{j+1}^{p+1} + D_5\alpha_{j+2}^{p+1}\\ &\quad - D_6\beta_{j-2}^{p+1} - D_7\beta_{j-1}^{p+1} + D_7\beta_{j+1}^{p+1} + D_6\beta_{j+2}^{p+1}\\ &= D_8\alpha_{j-2}^p + 26D_8\alpha_{j-1}^p + 66D_8\alpha_j^p + 26D_8\alpha_{j+1}^p + D_8\alpha_{j+2}^p\\ &\quad + D_6\beta_{j-2}^p + D_7\beta_{j-1}^p - D_7\beta_{j+1}^p - D_6\beta_{j+2}^p\\ &\quad - C\sum_{s=0}^{p}A_s((\alpha_{j-2}^{p-s+1} - \alpha_{j-2}^{p-s}) + 26(\alpha_{j-1}^{p-s+1} - \alpha_{j-1}^{p-s})\\ &\quad + 66(\alpha_j^{p-s+1} - \alpha_j^{p-s}) + 26(\alpha_{j+1}^{p-s+1} - \alpha_{j+1}^{p-s})\\ &\quad + (\alpha_{j+2}^{p-s+1} - \alpha_{j+2}^{p-s})) + (Q_1)_j^{p+1},\end{aligned} \tag{5.8}$$

$$\begin{aligned}&E_1\beta_{j-2}^{p+1} + E_2\beta_{j-1}^{p+1} + E_3\beta_j^{p+1} + E_4\beta_{j+1}^{p+1} + E_5\beta_{j+2}^{p+1} + E_6\alpha_{j-2}^{p+1}\\ &\quad + E_7\alpha_{j-1}^{p+1} + E_8\alpha_{j+1}^{p+1} + E_9\alpha_{j+2}^{p+1}\\ &= D_8\beta_{j-2}^p + 26D_8\beta_{j-1}^p + D_8\beta_j^p + 26D_8\beta_{j+1}^p + D_8\beta_{j+2}^p\\ &\quad + E_{10}\alpha_{j-2}^p - 2E_{10}\alpha_{j-1}^p + 2E_{10}\alpha_{j+1}^p - E_{10}\alpha_{j+2}^p\\ &\quad - C\sum_{s=0}^{p}A_s((\beta_{j-2}^{p-s+1} - \beta_{j-2}^{p-s}) + 26(\beta_{j-1}^{p-s+1} - \beta_{j-1}^{p-s})\\ &\quad + 66(\beta_j^{p-s+1} - \beta_j^{p-s}) + 26(\beta_{j+1}^{p-s+1} - \beta_{j+1}^{p-s})\\ &\quad + (\beta_{j+2}^{p-s+1} - \beta_{j+2}^{p-s})) + (Q_2)_j^{p+1},\end{aligned} \tag{5.9}$$

where

$$\begin{aligned}&D_1 = CA_0 + \frac{b_1}{2}z_2 - \frac{5b_1}{2h}z_1,\\ &D_2 = 26CA_0 + 13b_1z_2 - \frac{25b_1}{h}z_1,\\ &D_3 = 66CA_0 + 33b_1z_2,\\ &D_4 = 26CA_0 + 13b_1z_2 + \frac{25b_1}{h}z_1,\\ &D_5 = CA_0 + \frac{b_1}{2}z_2 + \frac{5b_1}{2h}z_1,\\ &D_6 = \frac{5a_1}{2h},\ D_7 = \frac{25a_1}{h},\ D_8 = CA_0,\\ &E_1 = CA_0 - \frac{5b_2}{2h}z_1,\\ &E_2 = 26CA_0 - \frac{25b_2}{h}z_1,\\ &E_3 = 66CA_0,\\ &E_4 = 26CA_0 + \frac{25b_2}{h}z_1,\\ &E_5 = CA_0 + \frac{5b_2}{2h}z_1,\\ &E_6 = -\frac{30a_2}{h^3} - \frac{5b_2}{2h}z_2,\\ &E_7 = \frac{60a_2}{h^3} - \frac{25b_2}{h}z_2,\\ &E_8 = -\frac{60a_2}{h^3} + \frac{25b_2}{h}z_2,\\ &E_9 = \frac{30a_2}{h^3} + \frac{5b_2}{2h}z_2,\\ &E_{10} = \frac{30a_2}{h^3},\\ &z_1 = \alpha_{j-2}^p + 26\alpha_{j-1}^p + 66\alpha_j^p + 26\alpha_{j+1}^p + \alpha_{j+2}^p,\\ &z_2 = \alpha_{j+2}^p + \alpha_{j+1}^p - 10\alpha_{j-1}^p - \alpha_{j-2}^p,\\ &z_3 = \beta_{j-2}^p + 26\beta_{j-1}^p + 66\beta_j^p + 26\beta_{j+1}^p + \beta_{j+2}^p,\\ &z_4 = \beta_{j+2}^p + \beta_{j+1}^p - 10\beta_{j-1}^p - \beta_{j-2}^p.\end{aligned}$$

Matrix form of Eqs. (5.8) and (5.9) becomes:

$$\begin{aligned}EF^{p+1} = GF^p - H\Bigg(&CA_p\alpha^0 + \sum_{s=0}^{p-1}(A_s - A_{s+1})\alpha^{s-p}\\ &+ CA_p\beta^0 + \sum_{s=0}^{p-1}(A_s - A_{s+1})\beta^{s-p}\Bigg) + q^{p+1}.\end{aligned} \tag{5.10}$$

After some simplification, we obtain

$$EF^{p+1} = I. \tag{5.11}$$

Here, the square matrix of order $(2N + 10) \times (2N + 10)$ is denoted by E. The column vector I consists of the order $(2N + 10)$ and $F^{p+1} = [\alpha_{-2}^{p+1}, \alpha_{-1}^{p+1}, \ldots, \beta_{N+2}^{p+1}, \beta_{-2}^{p+1}, \beta_{-1}^{p+1}, \ldots, \beta_{N+2}^{p+1}]^T$ contains the control points.

$$E = \begin{pmatrix} F_1 & \vdots & F_2 \\ \cdots & \cdots & \cdots \\ F_3 & \vdots & F_4 \end{pmatrix}, \quad G = \begin{pmatrix} F_5 & \vdots & F_6 \\ \cdots & \cdots & \cdots \\ F_6 & \vdots & F_5 \end{pmatrix},$$

$$H = \begin{pmatrix} F_8 & \vdots & F_6 \\ \cdots & \cdots & \cdots \\ F_6 & \vdots & F_8 \end{pmatrix}, \quad q^{p+1} = \begin{pmatrix} q_1 \\ \cdots \\ q_2 \end{pmatrix},$$

where

$$F_1 = \begin{pmatrix} 1 & 26 & 66 & 26 & 1 & & & & & \\ \frac{-5}{h} & \frac{-50}{h} & 0 & \frac{50}{h} & \frac{5}{h} & & & & & \\ D_1 & D_2 & D_3 & D_4 & D_5 & & & & & \\ & D_1 & D_2 & D_3 & D_4 & D_5 & & & & \\ & & \ddots & \ddots & \ddots & & & & & \\ & & & & \ddots & \ddots & \ddots & & & \\ & & & D_1 & D_2 & D_3 & D_4 & D_5 & & \\ & & & & D_1 & D_2 & D_3 & D_4 & D_5 & \\ & & & & \frac{-5}{h} & \frac{-50}{h} & 0 & \frac{50}{h} & \frac{5}{h} & \\ & & & & 1 & 26 & 66 & 26 & 1 & \end{pmatrix},$$

$$F_2 = \begin{pmatrix} 0 & 0 & 0 & 0 & 0 & & & & & \\ 0 & 0 & 0 & 0 & 0 & & & & & \\ -D_6 & -D_7 & 0 & D_7 & D_6 & & & & & \\ & -D_6 & -D_7 & 0 & D_7 & D_6 & & & & \\ & & \ddots & \ddots & \ddots & & & & & \\ & & & & \ddots & \ddots & \ddots & & & \\ & & & -D_6 & -D_7 & 0 & D_7 & D_6 & & \\ & & & & -D_6 & -D_7 & 0 & D_7 & D_6 & \\ & & & & 0 & 0 & 0 & 0 & 0 & \\ & & & & 0 & 0 & 0 & 0 & 0 & \end{pmatrix},$$

$$F_3 = \begin{pmatrix} 0 & 0 & 0 & 0 & 0 & & & & & \\ 0 & 0 & 0 & 0 & 0 & & & & & \\ E_1 & E_2 & E_3 & E_4 & E_5 & & & & & \\ & E_1 & E_2 & E_3 & E_4 & E_5 & & & & \\ & & \ddots & \ddots & \ddots & & & & & \\ & & & & \ddots & \ddots & \ddots & & & \\ & & & E_1 & E_2 & E_3 & E_4 & E_5 & & \\ & & & & E_1 & E_2 & E_3 & E_4 & E_5 & \\ & & & & 0 & 0 & 0 & 0 & 0 & \\ & & & & 0 & 0 & 0 & 0 & 0 & \end{pmatrix},$$

$$F_4 = \begin{pmatrix} 1 & 26 & 66 & 26 & 1 & & & & & \\ \frac{-5}{h} & \frac{-50}{h} & 0 & \frac{50}{h} & \frac{5}{h} & & & & & \\ E_6 & E_7 & 0 & E_8 & E_9 & & & & & \\ & E_6 & E_7 & 0 & E_8 & E_9 & & & & \\ & & \ddots & \ddots & \ddots & & & & & \\ & & & & \ddots & \ddots & \ddots & & & \\ & & & E_6 & E_7 & 0 & E_8 & E_9 & & \\ & & & & E_6 & E_7 & 0 & E_8 & E_9 & \\ & & & & \frac{-5}{h} & \frac{-50}{h} & 0 & \frac{50}{h} & \frac{5}{h} & \\ & & & & 1 & 26 & 66 & 26 & 1 & \end{pmatrix},$$

$$Z_5 = \begin{pmatrix} 0 & 0 & 0 & 0 & 0 & & & & & \\ 0 & 0 & 0 & 0 & 0 & & & & & \\ D_8 & 26D_8 & 66D_8 & 26D_8 & D_8 & & & & & \\ & D_8 & 26D_8 & 66D_8 & 26D_8 & D_8 & & & & \\ & & \ddots & \ddots & \ddots & & & & & \\ & & & & \ddots & \ddots & \ddots & & & \\ & & & D_8 & 26D_8 & 66D_8 & 26D_8 & D_8 & & \\ & & & & D_8 & 26D_8 & 66D_8 & 26D_8 & D_8 & \\ & & & & 0 & 0 & 0 & 0 & 0 & \\ & & & & 0 & 0 & 0 & 0 & 0 & \end{pmatrix},$$

$$Z_6 = \begin{pmatrix} 0 & 0 & 0 & 0 & 0 & & & & & \\ 0 & 0 & 0 & 0 & 0 & & & & & \\ 0 & 0 & 0 & 0 & 0 & & & & & \\ & 0 & 0 & 0 & 0 & 0 & & & & \\ & & \ddots & \ddots & \ddots & & & & & \\ & & & & \ddots & \ddots & \ddots & & & \\ & & & 0 & 0 & 0 & 0 & 0 & & \\ & & & & 0 & 0 & 0 & 0 & 0 & \\ & & & & 0 & 0 & 0 & 0 & 0 & \\ & & & & 0 & 0 & 0 & 0 & 0 & \end{pmatrix},$$

$$Z_7 = \begin{pmatrix} 0 & 0 & 0 & 0 & 0 & & & & & \\ 0 & 0 & 0 & 0 & 0 & & & & & \\ E_{10} & 26E_{10} & 66E_{10} & 26E_{10} & D_8 & & & & & \\ & B_9 & B_{10} & B_3 & B_{11} & B_{12} & & & & \\ & & \ddots & \ddots & \ddots & & & & & \\ & & & & \ddots & \ddots & \ddots & & & \\ & & & B_9 & B_{10} & B_3 & B_{11} & B_{12} & & \\ & & & & B_9 & B_{10} & B_3 & B_{11} & B_{12} & \\ & & & & 0 & 0 & 0 & 0 & 0 & \\ & & & & 0 & 0 & 0 & 0 & 0 & \end{pmatrix},$$

$$q_1 = \begin{pmatrix} g_1^{p+1} \\ g_3^{p+1} \\ (Q_1)_0^{p+1} \\ (Q_1)_1^{p+1} \\ \vdots \\ (Q_1)_{N-1}^{p+1} \\ (Q_1)_N^{p+1} \\ g_4^{p+1} \\ g_2^{p+1} \end{pmatrix}, \quad q_2 = \begin{pmatrix} h_1^{p+1} \\ h_3^{p+1} \\ (Q_1)_0^{p+1} \\ (Q_1)_1^{p+1} \\ \vdots \\ (Q_1)_{N-1}^{p+1} \\ (Q_1)_N^{p+1} \\ h_4^{p+1} \\ h_2^{p+1} \end{pmatrix},$$

$$Z_8 = \begin{pmatrix} 0 & 0 & 0 & 0 & 0 & & & & & \\ 0 & 0 & 0 & 0 & 0 & & & & & \\ 1 & 26 & 66 & 26 & 1 & & & & & \\ & 1 & 26 & 66 & 26 & 1 & & & & \\ & & \ddots & \ddots & \ddots & & & & & \\ & & & & \ddots & \ddots & \ddots & & & \\ & & & 1 & 26 & 66 & 26 & 1 & & \\ & & & & 1 & 26 & 66 & 26 & 1 & \\ & & & & 0 & 0 & 0 & 0 & 0 & \\ & & & & 0 & 0 & 0 & 0 & 0 & \end{pmatrix}.$$

6 Initial state

Initial vectors μ_j^0 and ν_j^0 have been calculated from the ICs. To start iteration on Eqs. (5.8) and (5.9), a suitable initial vector $F^0 = [\alpha_{-2}^0, \alpha_{-1}^0, \ldots, \beta_{N+2}^0, \beta_{-2}^0, \beta_{-1}^0, \ldots, \beta_{N+2}^{p+1}]^T$ can be calculated. The determination of the initial state is achieved by employing the ICs and their derivatives at the boundaries in a specific manner:

$$\begin{cases} (U_x)_{(x_0,0)} = -d_1\alpha_{-2}^0 - 10d_1\alpha_{-1}^0 + 10d_1\alpha_1^0 + d_1\alpha_2^0, \\ (U_{xx})_{(x_0,0)} = d_2\alpha_{-2}^0 + 2d_2\alpha_{-1}^0 - 6d_2\alpha_0^0 + 2d_2\alpha_1^0 + d_2\alpha_2^0, \\ (U)_{(x_j,0)} = \alpha_{j-2}^0 + 26\alpha_{j-1}^0 + 66\alpha_j^0 + 26\alpha_{j+1}^0 + \alpha_{j+2}^0, \\ (U_{xx})_{(x_N,0)} = d_2\alpha_{N-2}^0 + 2d_2\alpha_{N-1}^0 - 6d_2\alpha_N^0 + 2d_2\alpha_{N+1}^0 + d_2\alpha_{N+2}^0, \\ (U_x)_{(x_N,0)} = -d_1\alpha_{N-2}^0 - 10d_1\alpha_{N-1}^0 + 10d_1\alpha_{N+1}^0 + d_1\alpha_{N+2}^0, \\ (V_x)_{(x_0,0)} = -d_1\beta_{-2}^0 - 10d_1\beta_{-1}^0 + 10d_1\beta_1^0 + d_1\beta_2^0, \\ (V_{xx})_{(x_0,0)} = d_2\beta_{-2}^0 + 2d_2\beta_{-1}^0 - 6d_2\beta_0^0 + 2d_2\beta_1^0 + d_2\beta_2^0, \\ (U)_{(x_j,0)} = \beta_{j-2}^0 + 26\beta_{j-1}^0 + 66\beta_j^0 + 26\beta_{j+1}^0 + \beta_{j+2}^0, \\ (V_{xx})_{(x_N,0)} = d_2\beta_{N-2}^0 + 2d_2\beta_{N-1}^0 - 6d_2\beta_N^0 + 2d_2\beta_{N+1}^0 + d_2\beta_{N+2}^0, \\ (V_x)_{(x_N,0)} = -d_1\beta_{N-2}^0 - 10d_1\beta_{N-1}^0 + 10d_1\beta_{N+1}^0 + d_1\beta_{N+2}^0. \end{cases}$$

The matrix form for the aforementioned system is given as follows:

$$AF^0 = E, \tag{6.1}$$

where

$$A = \begin{pmatrix} P_1 & \vdots & Z_6 \\ \cdots & \cdots & \cdots \\ Z_6 & \vdots & P_1 \end{pmatrix}, E = \begin{pmatrix} E_1 \\ \cdots \\ E_2 \end{pmatrix},$$

where

$$P_1 = \begin{pmatrix} -\frac{5}{h} & -\frac{50}{h} & 0 & \frac{50}{h} & \frac{5}{h} & & & & & \\ \frac{20}{h^2} & \frac{40}{h^2} & -\frac{120}{h^2} & \frac{40}{h^2} & \frac{20}{h^2} & & & & & \\ 1 & 26 & 66 & 26 & 1 & & & & & \\ & 1 & 26 & 66 & 26 & 1 & & & & \\ & & \ddots & \ddots & \ddots & & & & & \\ & & & 1 & 26 & 66 & 26 & 1 & & \\ & & & & 1 & 26 & 66 & 26 & 1 & \\ & & & & \frac{20}{h^2} & \frac{40}{h^2} & -\frac{120}{h^2} & \frac{40}{h^2} & \frac{20}{h^2} & \\ & & & & -\frac{5}{h} & -\frac{50}{h} & 0 & \frac{50}{h} & \frac{5}{h} & \end{pmatrix},$$

$$E_1 = \begin{pmatrix} g'(c) \\ g''(c) \\ g(x_0) \\ g(x_1) \\ \vdots \\ g(x_{N-1}) \\ g(x_N) \\ g''(d) \\ g'(d) \end{pmatrix}, \quad E_2 = \begin{pmatrix} h'(c) \\ h''(c) \\ h(x_0) \\ h(x_1) \\ \vdots \\ h(x_{N-1}) \\ h(x_N) \\ h''(d) \\ h'(d) \end{pmatrix}.$$

7 Algorithm

Numerical solution of time fractional partial difference equation can be obtained using B-spline functions, if someone goes to following steps:

- Proceed by establishing the TFCBBE model.
- Set up effective techniques to discretize the spatial domain and time domain like Caputo function and piecewise QBS basis function.
- For each time step, the linear system is set up and matrices of order $(2N + 10) \times (2N + 10)$ are constructed.
- For each time step, we solve the system in question using Mathematica 13.2.

8 Stability analysis

Stability analysis is associated with computational method errors that exhibit no growth with the advancement of the technique. An algorithm is considered unconditionally stable when errors in a scheme still bounded. A stability study is shown to confirm that errors are not amplified by the scheme. There is a close relationship between the numerical scheme's stability and numerical error. The

principle of stability is linked to defects in computing techniques that never increase as the approach advances [47]. In this section, we use Fourier series technique to evaluate the stability of the proposed methodology [48]. The non-linear terms are temporarily frozen to conduct stability analyzis. Consequently, U and V have been frozen as constants ω_1 and ω_2, respectively [49]. Stability analyzis is only suitable for linear equations. By replacing an approximation of the equation, the subsequent Eqs. (5.6) and (5.7) are developed:

$$\begin{aligned} CA_0U_j^{p+1} + \frac{b_1}{2}\omega_1(U_x)_j^{p+1} + \frac{a_1}{2}(V_x)_j^{p+1} &= CA_0U_j^p - \frac{b_1}{2}\omega_1(U_x)_j^p - \frac{a_1}{2}(V_x)_j^p \\ &\quad - C\sum_{s=1}^{p}A_s(U_j^{p-s+1} - U_j^{p-s}) + Q_1, \end{aligned} \tag{8.1}$$

$$\begin{aligned} &CA_0V_j^{p+1} + \frac{b_2}{2}\omega_1(V_x)_j^{p+1} + \frac{b_2}{2}\omega_2(U_x)_j^{p+1} + \frac{a_2}{2}\theta(U_{xxx})_j^{p+1} \\ &= CA_0V_j^p - \frac{b_2}{2}\omega_1(V_x)_j^p - \frac{b_2}{2}\omega_2(U_x)_j^p - \frac{a_2}{2}\theta(U_{xxx})_j^p \\ &\quad - C\sum_{s=1}^{p}A_s(V_j^{p-s+1} - V_j^{p-s}) + Q_2. \end{aligned} \tag{8.2}$$

Consider $\tilde{u}_j^p$ and $\tilde{v}_j^p$ are the approximated solution of (8.1) and (8.2) with errors α_j^p and β_j^p, which are defined as follows:

$$\begin{cases} \alpha_j^p = U_j^p - \tilde{u}_j^p, \\ \beta_j^p = V_j^p - \tilde{v}_j^p, \end{cases} \tag{8.3}$$

where $p = 0, 1, \ldots, M$, and $j = 0, 1, \ldots N-1$, using QBS basis function, Eqs. (8.1) and (8.2) becomes:

$$\begin{aligned} &\left(CA_0 - \frac{5b_1\omega_1}{2h}\right)\alpha_{j-2}^{p+1} + \left(26CA_0 - \frac{25b_1\omega_1}{h}\right)\alpha_{j-1}^{p+1} \\ &\quad + (66CA_0)\alpha_j^{p+1} + \left(26CA_0 + \frac{25b_1\omega_1}{h}\right)\alpha_{j+1}^{p+1} \\ &\quad + \left(CA_0 + \frac{5b_1\omega_1}{2h}\right)\alpha_{j+2}^{p+1} - \frac{5a_1}{2h}\beta_{j-2}^{p+1} \\ &\quad - \frac{25a_1}{h}\beta_{j-1}^{p+1} + \frac{25a_1}{h}\beta_{j+1}^{p+1} + \frac{5a_1}{2h}\beta_{j+2}^{p+1} \\ &= \left(CA_0 + \frac{5b_1\omega_1}{2h}\right)\alpha_{j-2}^{p} + \left(26CA_0 + \frac{25b_1\omega_1}{h}\right)\alpha_{j-1}^{p} \\ &\quad + (66CA_0)\alpha_j^{p} + \left(26CA_0 - \frac{25b_1\omega_1}{h}\right)\alpha_{j+1}^{p} \\ &\quad + \left(CA_0 - \frac{5b_1\omega_1}{2h}\right)\alpha_{j+2}^{p} + \frac{5a_1}{2h}\beta_{j-2}^{p} + \frac{25a_1}{h}\beta_{j-1}^{p} \\ &\quad - \frac{25a_1}{h}\beta_{j+1}^{p} - \frac{5a_1}{2h}\beta_{j+2}^{p} - C\sum_{s=0}^{p}A_s((\alpha_{j-2}^{p-s+1} - \alpha_{j-2}^{p-s}) \\ &\quad + 26(\alpha_{j-1}^{p-s+1} - \alpha_{j-1}^{p-s}) + 66(\alpha_j^{p-s+1} - \alpha_j^{p-s}) \\ &\quad + 26(\alpha_{j+1}^{p-s+1} - \alpha_{j+1}^{p-s}) + (\alpha_{j+2}^{p-s+1} - \alpha_{j+2}^{p-s})), \end{aligned} \tag{8.4}$$

$$\begin{aligned} &\left(CA_0 - \frac{5b_2\omega_1}{2h}\right)\beta_{j-2}^{p+1} + \left(26CA_0 - \frac{25b_2\omega_1}{h}\right)\beta_{j-1}^{p+1} + (66CA_0)\beta_j^{p+1} \\ &\quad + \left(26CA_0 + \frac{25b_2\omega_1}{h}\right)\beta_{j+1}^{p+1} + \left(CA_0 + \frac{5b_2\omega_1}{2h}\right)\beta_{j+2}^{p+1} \\ &\quad + \left(\frac{-5b_2\omega_2}{2h} - \frac{30a_2}{h^3}\right)\alpha_{j-2}^{p+1} + \left(\frac{-25b_2\omega_2}{h} + \frac{60a_2}{h^3}\right)\alpha_{j-1}^{p+1} \\ &\quad + \left(\frac{25b_2\omega_2}{h} - \frac{60a_2}{h^3}\right)\alpha_{j+1}^{p+1} + \left(\frac{5b_2\omega_2}{2h} + \frac{30a_2}{h^3}\right)\alpha_{j+2}^{p+1} \\ &= \left(CA_0 + \frac{5b_2\omega_1}{2h}\right)\beta_{j-2}^{p} + \left(26CA_0 + \frac{25b_2\omega_1}{h}\right)\beta_{j-1}^{p} \\ &\quad + (66CA_0)\beta_j^{p} + \left(26CA_0 - \frac{25b_2\omega_1}{h}\right)\beta_{j+1}^{p} \\ &\quad + \left(CA_0 - \frac{5b_2\omega_1}{2h}\right)\beta_{j+2}^{p} + \left(\frac{5b_2\omega_2}{2h} + \frac{30a_2}{h^3}\right)\alpha_{j-2}^{p} \\ &\quad + \left(\frac{25b_2\omega_2}{h} - \frac{60a_2}{h^3}\right)\alpha_{j-1}^{p} + \left(\frac{-25b_2\omega_2}{h} + \frac{60a_2}{h^3}\right)\alpha_{j+1}^{p} \\ &\quad + \left(\frac{-5b_2\omega_2}{2h} - \frac{30a_2}{h^3}\right)\alpha_{j+2}^{p} - C\sum_{s=0}^{p}A_s((\beta_{j-2}^{p-s+1} - \beta_{j-2}^{p-s}) \\ &\quad + 26(\beta_{j-1}^{p-s+1} - \beta_{j-1}^{p-s}) + 66(\beta_j^{p-s+1} - \beta_j^{p-s}) \\ &\quad + 26(\beta_{j+1}^{p-s+1} - \beta_{j+1}^{p-s}) + (\beta_{j+2}^{p-s+1} - \beta_{j+2}^{p-s})). \end{aligned} \tag{8.5}$$

Now consider the Fourier series [50] solution in difference expressions, which can be characterized as:

$$\begin{cases} \alpha_j^p = \tilde{A}_p e^{i\xi_x jh}, \\ \beta_j^p = \tilde{B}_p e^{i\xi_x jh}, \end{cases} \tag{8.6}$$

where $\xi_x = (2\pi\ell/L)$. Eqs. (8.7) and (8.8) can be obtained using Fourier series in (8.4) and (8.5):

$$\begin{aligned} &\tilde{A}_{p+1}\left(\left(CA_0 - \frac{5b_1\omega_1}{2h}\right)e^{-2i\xi_x h} + \left(26CA_0 - \frac{25b_1\omega_1}{h}\right)e^{-i\xi_x h} \right. \\ &\quad + 66CA_0 + \left(26CA_0 + \frac{25b_1\omega_1}{h}\right)e^{i\xi_x h} \\ &\quad \left. + \left(CA_0 + \frac{5b_1\omega_1}{2h}\right)e^{2i\xi_x h}\right) + \tilde{B}_{p+1}\left(-\frac{5a_1}{2h}e^{-2i\xi_x h}\right. \\ &\quad \left. - \frac{25a_1}{h}e^{-i\xi_x h} + \frac{25a_1}{h}e^{i\xi_x h} + \frac{5a_1}{2h}e^{2i\xi_x h}\right) \\ &= \tilde{A}_p\left(\left(CA_0 + \frac{5b_1\omega_1}{2h}\right)e^{-2i\xi_x h} + \left(26CA_0\right.\right. \\ &\quad \left.\left. + \frac{25b_1\omega_1}{h}\right)e^{-i\xi_x h} + 66CA_0 + \left(26CA_0\right.\right. \\ &\quad \left.\left. - \frac{25b_1\omega_1}{h}\right)e^{i\xi_x h} + \left(CA_0 - \frac{5b_1\omega_1}{2h}\right)e^{2i\xi_x h}\right) \\ &\quad + \tilde{B}_p\left(+\frac{5a_1}{2h}e^{-2i\xi_x h} + \frac{25a_1}{h}e^{-i\xi_x h} - \frac{25a_1}{h}e^{i\xi_x h} - \frac{5a_1}{2h}e^{2i\xi_x h}\right) \\ &\quad - C\sum_{s=0}^{p}((\tilde{A}_{p-s+1} - \tilde{A}_{p-s})e^{-2i\xi_x h} + 26(\tilde{A}_{p-s+1} - \tilde{A}_{p-s})e^{-i\xi_x h} \\ &\quad + 66(\tilde{A}_{p-s+1} - \tilde{A}_{p-s}) + 26(\tilde{A}_{p-s+1} - \tilde{A}_{p-s})e^{i\xi_x h} \\ &\quad + (\tilde{A}_{p-s+1} - \tilde{A}_{p-s})e^{2i\xi_x h}), \end{aligned} \tag{8.7}$$

$$\begin{aligned}
&\tilde{B}_{p+1}\Big(\Big(CA_0 - \frac{5b_2\omega_1}{2h}\Big)e^{-2i\xi_x h} + \Big(26CA_0 - \frac{25b_2\omega_1}{h}\Big)e^{-i\xi_x h} \\
&\quad + (66CA_0) + \Big(26CA_0 + \frac{25b_2\omega_1}{h}\Big)e^{i\xi_x h} \\
&\quad + \Big(CA_0 + \frac{5b_2\omega_1}{2h}\Big)e^{2i\xi_x h}\Big) + \tilde{A}_{p+1}\Big(\Big(\frac{-5b_2\omega_2}{2h} - \frac{30a_2}{h^3}\Big)e^{-2i\xi_x h} \\
&\quad + \Big(\frac{-25b_2\omega_2}{h} + \frac{60a_2}{h^3}\Big)e^{-i\xi_x h} + \Big(\frac{25b_2\omega_2}{h} - \frac{60a_2}{h^3}\Big)e^{i\xi_x h} \\
&\quad + \Big(\frac{5b_2\omega_2}{2h} + \frac{30a_2}{h^3}\Big)e^{2i\xi_x h}\Big) \\
&= \tilde{B}_p\Big(\Big(CA_0 + \frac{5b_2\omega_1}{2h}\Big)e^{-2i\xi_x h} + \Big(26CA_0 + \frac{25b_2\omega_1}{h}\Big)e^{-i\xi_x h} \\
&\quad + (66CA_0) + \Big(26CA_0 - \frac{25b_2\omega_1}{h}\Big)e^{i\xi_x h} \\
&\quad + \Big(CA_0 - \frac{5b_2\omega_1}{2h}\Big)e^{2i\xi_x h}\Big) + \tilde{A}_p\Big(\Big(\frac{5b_2\omega_2}{2h} + \frac{30a_2}{h^3}\Big)e^{-2i\xi_x h} \\
&\quad + \Big(\frac{25b_2\omega_2}{h} - \frac{60a_2}{h^3}\Big)e^{-i\xi_x h} + \Big(\frac{-25b_2\omega_2}{h} + \frac{60a_2}{h^3}\Big)e^{i\xi_x h} \\
&\quad + \Big(\frac{-5b_2\omega_2}{2h} - \frac{30a_2}{h^3}\Big)e^{2i\xi_x h}\Big) - C\sum_{s=0}^{p}((\tilde{B}_{p-s+1} - \tilde{B}_{p-s})e^{-2i\xi_x h} \\
&\quad + 26(\tilde{B}_{p-s+1} - \tilde{B}_{p-s})e^{-i\xi_x h} + 66(\tilde{B}_{p-s+1} - \tilde{B}_{p-s}) \\
&\quad + 26(\tilde{B}_{p-s+1} - \tilde{B}_{p-s})e^{i\xi_x h} + (\tilde{B}_{p-s+1} - \tilde{B}_{p-s})e^{2i\xi_x h}).
\end{aligned} \tag{8.8}$$

Eqs. (8.9) and (8.10) can obtained by utilizing the relation $e^{i\xi_x h} + e^{-i\xi_x h} = 2\cos(\xi_x h)$ in Eqs. (8.7) and (8.8):

$$\begin{aligned}
&\tilde{A}_{p+1}((66CA_0 + 2CA_0\cos(2\xi_x h) + 52CA_0\cos(\xi_x h)) \\
&\quad + i\Big(\frac{5b_1\omega_1}{h}\sin(2\xi_x h) + \frac{50b_1\omega_1}{h}\sin(\xi_x h)\Big)\Big) \\
&\quad + \tilde{B}_{p+1}i\Big(\frac{5a_1}{h}\sin(2\xi_x h) + \frac{50a_1}{h}\sin(\xi_x h)\Big) \\
&= \tilde{A}_p((66CA_0 + 2CA_0\cos(2\xi_x h) + 52CA_0\cos(\xi_x h)) \\
&\quad - i\Big(\frac{5b_1\omega_1}{h}\sin(2\xi_x h) + \frac{50b_1\omega_1}{h}\sin(\xi_x h)\Big)\Big) \\
&\quad - \tilde{B}_p i\Big(\frac{5a_1\lambda}{h}\sin(2\xi_x h) + \frac{50a_1\lambda}{h}\sin(\xi_x h)\Big) \\
&\quad - C\sum_{s=0}^{p}((\tilde{A}_{p-s+1} - \tilde{A}_{p-s})(2\cos(2\xi_x h) \\
&\quad + 52\cos(\xi_x h) + 66)),
\end{aligned} \tag{8.9}$$

$$\begin{aligned}
&\tilde{B}_{p+1}((66CA_0 + 2CA_0\cos(2\xi_x h) + 52CA_0\cos(\xi_x h)) \\
&\quad + i\Big(\frac{5b_2\omega_1}{h}\sin(2\xi_x h) + \frac{50b_2\omega_1}{h}\sin(\xi_x h)\Big)\Big) \\
&\quad + \tilde{A}_{p+1}i\Big(-\frac{5b_2\omega_2}{2h}\sin(2\xi_x h) - \frac{30a_2}{h^3}\sin(2\xi_x h) \\
&\quad + \frac{50b_2\omega_2}{h}\sin(\xi_x h) - \frac{120a_2}{h^3}\sin(\xi_x h)\Big) \\
&= \tilde{B}_p((66CA_0 + 2CA_0\cos(2\xi_x h) + 52CA_0\cos(\xi_x h)) \\
&\quad - i\Big(\frac{5b_2\omega_1}{h}\sin(2\xi_x h) + \frac{50b_2\omega_1}{h}\sin(\xi_x h)\Big)\Big) \\
&\quad + \tilde{A}_p i\Big(-\frac{5b_2\omega_2}{2h}\sin(2\xi_x h) - \frac{30a_2}{h^3}\sin(2\xi_x h) \\
&\quad + \frac{50b_2\omega_2}{h}\sin(\xi_x h) - \frac{120a_2}{h^3}\sin(\xi_x h)\Big) \\
&\quad - C\sum_{s=0}^{p}((\tilde{B}_{p-s+1} - \tilde{B}_{p-s})(66 + 2\cos(2\xi_x h) \\
&\quad + 52\cos(\xi_x h))).
\end{aligned} \tag{8.10}$$

Taking $\tilde{U} = 66CA_0 + 2CA_0\cos(2\xi_x h) + 52CA_0\cos(\xi_x h)$,

$$\begin{aligned}
\tilde{V} &= \tfrac{5b_1\omega_1}{h}\sin(2\xi_x h) + \tfrac{50b_1\omega_1}{h}\sin(\xi_x h), \\
\tilde{W} &= \tfrac{5a_1\lambda}{h}\sin(2\xi_x h) + \tfrac{50a_1\lambda}{h}\sin(\xi_x h), \\
\tilde{X} &= 2\cos(2\xi_x h) + 52\cos(\xi_x h), \\
\tilde{Y} &= -\tfrac{5b_2\omega_2}{2h}\sin(2\xi_x h) - \tfrac{30a_2}{h^3}\sin(2\xi_x h) \\
&\quad + \tfrac{50b_2\omega_2}{h}\sin(\xi_x h) - \tfrac{120a_2}{h^3}\sin(\xi_x h).
\end{aligned}$$

Using the aforementioned abbreviations, Eq. (8.9) implies that

$$\begin{aligned}
&(\tilde{U} + i\tilde{V})\tilde{A}_{p+1} + i\tilde{W}\tilde{B}_{p+1} \\
&\quad = (\tilde{U} + i\tilde{V})\tilde{A}_p + i\tilde{W}\tilde{B}_p + \sum_{s=0}^{p}((\tilde{A}_{p-s+1} \\
&\quad - \tilde{A}_{p-s})\tilde{X} + 66),
\end{aligned} \tag{8.11}$$

$$\begin{aligned}
&(\tilde{U} + i\tilde{V})\tilde{A}_{p+1} \\
&\quad = (\tilde{U} + i\tilde{V})\tilde{A}_p - i\tilde{W}\tilde{B}_{p+1} - i\tilde{W}\tilde{B}_p \\
&\quad + \sum_{s=0}^{p}((\tilde{A}_{p-s+1} - \tilde{A}_{p-s})\tilde{X} + 66),
\end{aligned} \tag{8.12}$$

then

$$\begin{aligned}
|\tilde{A}_{p+1}| &\le |\tilde{A}_p| + \frac{|i\tilde{W}|}{|\tilde{U} + i\tilde{V}|}(|\tilde{B}_{p+1}| + |\tilde{B}_p|) \\
&\quad + \frac{1}{|\tilde{U} + i\tilde{V}|}\sum_{s=0}^{p}((\tilde{A}_{p-s+1} - \tilde{A}_{p-s})\tilde{X} + 66).
\end{aligned} \tag{8.13}$$

Similarly for Eq. (8.10).

Theorem 1. *If the solution of* (8.12) *is* $\tilde{A}_p$ *and* $\tilde{E}_p$ *represents a positive constant, then we have*

$$|\tilde{A}_p| \le \tilde{E}_p|\tilde{A}_0|, \quad \text{where } p = 1, 2, 3, \ldots, M-1. \tag{8.14}$$

Proof. To prove this result (8.13), we use induction method. Firstly, suppose for $p = 1$, then we have

$$|\tilde{A}_p| \le |\tilde{A}_0| + \frac{1}{|\tilde{U} + i\tilde{V}|}(|\tilde{B}_1| + |\tilde{B}_0|). \tag{8.15}$$

Using the convergence of the series, there exists a positive constant P, such that

$$|\tilde{B}_p| \le P|\tilde{A}_0|, p = 0, 1, 2, \ldots, M-1.$$

Eq. (8.15) becomes

$$|\tilde{A}_p| \le |\tilde{A}_0| + \tilde{P}_1|\tilde{A}_0| \le (1 + \tilde{P}_1)|\tilde{A}_0| \le \tilde{E}_1|\tilde{A}_0|,$$

where $\tilde{P}_1 = \frac{1}{|\tilde{U} + i\tilde{V}|}$ and $\tilde{E}_1 = 1 + \tilde{P}_1$. Second, suppose that

$$|\tilde{A}_p| \le \tilde{E}_1|\tilde{A}_0|, p = 1, 2, \ldots, M-2.$$

Eq. (8.13) provides

$$\begin{aligned} |\tilde{A}_{p+1}| &\le \tilde{E}_p|\tilde{A}_0| + \tilde{G}\tilde{E}_1|\tilde{A}_0| + \tilde{P}_1\sum_{s=1}^{p}((\tilde{A}_0 - \tilde{A}_0)\tilde{X}) \\ &\le \tilde{E}_{p+1}|\tilde{A}_0|, \end{aligned} \tag{8.16}$$

where $\tilde{G} = \frac{|i\tilde{W}|}{|\tilde{U} + i\tilde{V}|}$. □

Remark 1. Similar to the aforementioned pattern, we have

$$|\tilde{B}_p| \le I_p|\tilde{B}_0|, \quad p = 1, 2, \ldots, M-2, M-1. \tag{8.17}$$

Here, I_p is a positive constant.

9 Convergence analyzis

Theorem 2. *Let* U_j^p, *and* V_j^p *be the exact solutions, and* $\widetilde{U}_j^p$ *and* $\widetilde{V}_j^p$ *be the time-discrete values of the TFCBBE. Then,*

$$\begin{cases} \|\tilde{\alpha}^{p+1}\| \le G\tau^2, \\ \|\tilde{\beta}^{p+1}\| \le G\tau^2, \end{cases} \tag{9.1}$$

where $\tilde{\alpha}^{p+1} = U_j^p - \widetilde{U}_j^p$ *and* $\tilde{\beta}^{p+1} = V_j^p - \widetilde{V}_j^p$.

Proof. Let U and V be positive constants, and let $\widetilde{\chi}_1$ and $\widetilde{\chi}_2$ represent certain parameters in the analyzis. In this case, the linearized time-discrete solutions are as follows:

$$\begin{aligned} C\tilde{\alpha}^{p+1} + \frac{b_1}{2}\widetilde{\chi}_1(\tilde{\alpha}_x)^{p+1} + \frac{a_1}{2}(\widetilde{\beta}_x)^{p+1} \\ = C\tilde{\alpha}^p + C\sum_{s=0}^{p-1}[A_s - A_{s+1}]\tilde{\alpha}^{p-s} + Q_1^{p+1}. \end{aligned} \tag{9.2}$$

By substituting $p = 0$ in (9.2), we have

$$C\tilde{\alpha}^1 + \frac{b_1}{2}\widetilde{\chi}_1(\tilde{\alpha}_x)^1 + \frac{a_1}{2}(\widetilde{\beta}_x)^1 = C\tilde{\alpha}^0 + Q_1^1. \tag{9.3}$$

As $\tilde{\alpha}^0 = 0$, and taking inner product w.r.t $\tilde{\alpha}^1$, we obtain

$$C\langle\tilde{\alpha}^1, \tilde{\alpha}^1\rangle + \frac{b_1}{2}\widetilde{\chi}_1\langle\tilde{\alpha}_x^1, \tilde{\alpha}^1\rangle + \frac{a_1}{2}\langle\widetilde{\beta}_x^1, \alpha^1\rangle = \langle Q_1^1, \tilde{\alpha}^1\rangle. \tag{9.4}$$

We used

$$\begin{cases} \langle\tilde{\alpha}_{xxx}, \tilde{\alpha}\rangle = -\langle\tilde{\alpha}_{xx}, \tilde{\alpha}_{xx}\rangle, \\ \langle\tilde{\alpha}_{xx}, \tilde{\alpha}\rangle = -\langle\tilde{\alpha}_x, \tilde{\alpha}_x\rangle, \\ \langle\tilde{\alpha}, \tilde{\alpha}_x\rangle = -\langle\tilde{\alpha}_x, \tilde{\alpha}\rangle, \\ \langle\tilde{\alpha}, \tilde{\alpha}\rangle = \|\tilde{\alpha}\|^2, \\ \langle\tilde{\alpha}, \tilde{\alpha}^1\rangle \le \|\tilde{\alpha}\|\|\tilde{\alpha}^1\|. \end{cases} \tag{9.5}$$

$$C\langle\tilde{\alpha}^1, \tilde{\alpha}^1\rangle \le -\frac{b_1}{2}\widetilde{\chi}_1\langle\tilde{\alpha}_x^1, \tilde{\alpha}^1\rangle - \frac{a_1}{2}\langle\widetilde{\beta}_x^1, \alpha^1\rangle + \langle Q_1^1, \alpha^1\rangle.$$

$$W\|\alpha^1\|^2 \le \|Q_1^1\|\|\alpha^1\|,$$

and

$$\|\alpha^1\| \le G\tau^2. \tag{9.6}$$

Given that Eq. (9.6) is valid for values of p ranging from 0 to $M-1$. Next, by computing the inner product of Eq. (9.2) with α^{p+1}, we conclude

$$\begin{aligned} C\langle\tilde{\alpha}^{p+1}, \tilde{\alpha}^{p+1}\rangle + \frac{b_1}{2}\widetilde{\chi}_1\langle\tilde{\alpha}_x^{p+1}, \tilde{\alpha}^{p+1}\rangle + \frac{a_1}{2}\langle\widetilde{\beta}_x^{p+1}, \tilde{\alpha}^{p+1}\rangle \\ = C\langle\tilde{\alpha}^0, \tilde{\alpha}^{p+1}\rangle + C\sum_{s=0}^{p-1}[A_s - A_{s+1}]\langle\tilde{\alpha}^{p-s}, \tilde{\alpha}^{p+1}\rangle \\ + \langle Q_1^{p+1}, \tilde{\alpha}^{p+1}\rangle, \end{aligned}$$

$$\begin{aligned} C\langle\tilde{\alpha}^{p+1}, \tilde{\alpha}^{p+1}\rangle \le -\frac{b_1}{2}\widetilde{\chi}_1\langle\tilde{\alpha}_x^{p+1}, \tilde{\alpha}^{p+1}\rangle - \frac{a_1}{2}\langle\widetilde{\beta}_x^{p+1}, \tilde{\alpha}^{p+1}\rangle \\ + C\sum_{s=0}^{p-1}[A_s - A_{s+1}]\langle\tilde{\alpha}^{p-s}, \tilde{\alpha}^{p+1}\rangle + \langle Q_1^{p+1}, \tilde{\alpha}^{p+1}\rangle, \end{aligned}$$

$$C\|\tilde{\alpha}^{p+1}\|^2 \le C\sum_{s=0}^{p-1}[A_s - A_{s+1}]\|\tilde{\alpha}^{p-s}\|\|\tilde{\alpha}^{p+1}\| + \|Q_1^{p+1}\|\|\tilde{\alpha}^{p+1}\|,$$

$$\|\tilde{\alpha}^{p+1}\| \le \sum_{s=0}^{p-1}[A_s - A_{s+1}]\|\tilde{\alpha}^{p-s}\| + \frac{\|Q_1^{p+1}\|}{C},$$

$$\begin{aligned} \|\tilde{\alpha}^{p+1}\| \le [A_0 - Z_1]\|\tilde{\alpha}^p\| + [A_1 - A_2]\|\tilde{\alpha}^{p-1}\| \\ + \ldots + [A_{p-1} - A_p]\|\tilde{\alpha}^1\| + \frac{\|Q_1^{p+1}\|}{C}, \end{aligned}$$

$$\|\tilde{\alpha}^{p+1}\| \le G_0\tau^2 + G_1\tau^2 + \ldots + G_{p-1}\tau^2 + G_p\tau^2,$$
$$\|\tilde{\alpha}^{p+1}\| \le G\tau^2, \tag{9.7}$$

where $G_0, G_1, \ldots, G_p$ are constants independent of τ. Similarly, we can proof it for (5.7). □

10 Illustration of numerical examples and discussion

Numerical results are presented in this section to verify the accuracy of the scheme using the error norms L_2 and L_∞ [44], i.e.,

$$L_\infty(N) = \|U(x_i, t) - \tilde{U}(x_i, t)\|_\infty = \max|U(x_i, t) - \tilde{U}(x_i, t)|$$

and

$$L_2(N) = \|U(x_i, t) - \tilde{U}(x_i, t)\|_2 = \left(h\sum_{i=0}^{N}|U(x_i, t) - \tilde{U}(x_i, t)|^2\right)^{\frac{1}{2}}.$$

Example 10.1. Take the TFCBBE with Caputo sense, when $a_1 = a_2 = -1/2$ and $b_1 = b_2 = 2$,

$$\begin{cases} \dfrac{\partial^\lambda U(x,t)}{\partial t^\lambda} + a_1\dfrac{\partial V(x,t)}{\partial x} + b_1U(x,t)\dfrac{\partial U(x,t)}{\partial x} \\ \quad = Q_1(x,t), \\ \dfrac{\partial^\lambda V(x,t)}{\partial t^\lambda} + a_2\dfrac{\partial^3 U(x,t)}{\partial x^3} + b_2\dfrac{\partial(U(x,t)V(x,t))}{\partial x} \\ \quad = Q_2(x,t), \end{cases} \tag{10.1}$$
$$-25 \le x \le 25,\ 0 \le t \le 1,\ 0 < \lambda < 1.$$

with ICs

$$\begin{cases} U(x,0) = 1 + \left(0\tanh\dfrac{x}{2}\right)^2 = 1, \\ V(x,0) = \dfrac{1}{2}\left(0\,\mathrm{sech}\dfrac{x}{2}\right)^2 = 0, \end{cases}$$

and BCs

$$\begin{cases} U(a,t) = 1 + \left(t\tanh\dfrac{-25}{2}\right)^2, \\ V(a,t) = \dfrac{1}{2}\left(t\,\mathrm{sech}\dfrac{-25}{2}\right)^2, \\ U(b,t) = 1 + \left(t\tanh\dfrac{-25}{2}\right)^2, \\ V(b,t) = \dfrac{1}{2}\left(t\,\mathrm{sech}\dfrac{25}{2}\right)^2, \\ U_x(a,t) = t^2\tanh\dfrac{-25}{2}\left(\mathrm{sech}\dfrac{-25}{2}\right)^2, \\ V_x(a,t) = -\dfrac{1}{2}t^2\left(\mathrm{sech}\dfrac{-25}{2}\right)^2\tanh\dfrac{-25}{2}, \\ U_x(b,t) = t^2\tanh\dfrac{25}{2}\left(\mathrm{sech}\dfrac{25}{2}\right)^2, \\ V_x(b,t) = -\dfrac{1}{2}t^2\left(\mathrm{sech}\dfrac{25}{2}\right)^2\tanh\dfrac{25}{2}. \end{cases} \tag{10.2}$$

The exact solutions $U(x,t) = 1 + \left(t\tanh\frac{x}{2}\right)^2$ and $V(x,t) = \frac{1}{2}\left(t\,\mathrm{sech}\frac{x}{2}\right)^2$ are taken for comparison purpose between numerical solutions.

Tables 2–4 present the comparison between the exact and approximate solutions, along with the error norms for solution $U(x,t)$ at various stages of λ, when the parameters

Table 2: Comparison between exact and approximate solutions $U(x,t)$ at x and λ, for example 10.1 with error norms, at $T = 0.05$, $N = 100$, and $\tau = 0.002$

x	Exact solution	Approximate solutions			
		$\lambda = 0.3$	$\lambda = 0.5$	$\lambda = 0.7$	$\lambda = 0.9$
−25	1.0025	1.0025	1.0025	1.0025	1.0025
−20	1.0025	1.0025	1.0025	1.0025	1.0025
−15	1.0025	1.0025	1.0025	1.0025	1.0025
−10	1.0025	1.0025	1.0025	1.0025	1.0025
−5	1.00243	1.00243	1.00243	1.00243	1.00244
0	1	1	1	1	1
5	1.00243	1.00243	1.00243	1.00243	1.00244
10	1.0025	1.0025	1.0025	1.0025	1.0025
15	1.0025	1.0025	1.0025	1.0025	1.0025
20	1.0025	1.0025	1.0025	1.0025	1.0025
25	1.0025	1.0025	1.0025	1.0025	1.0025
L_∞	⋯	1.26147×10^{-7}	2.96880×10^{-7}	1.16733×10^{-6}	4.40604×10^{-6}
L_2	⋯	2.22257×10^{-7}	8.58436×10^{-7}	3.76634×10^{-6}	4.77101×10^{-6}

Table 3: Comparison between exact and approximate solution $U(x,t)$ at x and λ, for example 10.1 with error norms, at $T = 0.1$, $N = 100$, and $\tau = 0.002$

x	Exact solution	Approximate solutions			
		$\lambda = 0.2$	$\lambda = 0.4$	$\lambda = 0.6$	$\lambda = 0.8$
−25	1.01	1.01	1.01	1.01	1.01
−20	1.01	1.01	1.01	1.01	1.01
−15	1.01	1.01	1.01	1.01	1.01
−10	1.01	1.01	1.01	1.01	1.01
−5	1.00973	1.00973	1.00973	1.00974	1.00974
0	1	0.999999	1	1	1
5	1.00984	1.00973	1.00973	1.00974	1.00974
10	1.01	1.01	1.01	1.01	1.01
15	1.01	1.01	1.01	1.01	1.01
20	1.01	1.01	1.01	1.01	1.01
25	1.01	1.01	1.01	1.01	1.01
L_∞	⋯	5.78594×10^{-7}	5.48346×10^{-7}	3.23546×10^{-6}	1.02358×10^{-5}
L_2	⋯	7.30939×10^{-7}	1.67183×10^{-6}	7.80016×10^{-6}	3.20482×10^{-5}

are $N = 100$ and $\tau = 0.002$ at different values of $T = 0.05$, $T = 0.1$ and $T = 0.3$, respectively. Tables 5–7 present the comparison between the exact and approximate solutions, along with the error norms for solution $V(x,t)$ at various stages of λ, with parameters $N = 100$, $\tau = 0.002$ at various time levels $T = 0.05, T = 0.1$, and $T = 0.3$, respectively. Tables 8 and 9 represent the comparison between exact and approximate solutions, as well as their absolute errors, at various stages of x, with Table 8 concentrating on solution $U(x,t)$, while Table 9 on solution $V(x,t)$. The order of convergence is shown in Table 10 for different value of N with $\lambda = 0.3$ and $\tau = 0.002$. Figure 1 shows the $3D$ graphs of the exact and approximate solutions of functions with $N = 50$, $\lambda = 0.55$, and $\tau = 0.002$. Figure 2 shows the $2D$ comparison between the exact and approximate solutions of functions with $N = 50, \lambda = 0.55$, and $\tau = 0.002$, which demonstrate the effectiveness, reliability, and accuracy of the proposed method. Contour plots are presented in Figure 3, which represents the error value under the relation between x and t, $N = 100$, $\lambda = 0.5$, and $\tau = 0.01$. The graphically comparison between exact and approximate solutions is presented in Figure 4 at various time levels, $N = 100$, $\lambda = 0.3$, and $\tau = 0.01$, which demonstrate the convergence behavior on solution by changing parameter.

Example 10.2. Take the TFCBBE with Caputo sense, when $a_1 = a_2 = -1/2$ and $b_1 = b_2 = 2$,

Table 4: Comparison between exact and approximate solution $U(x,t)$ at x and λ, for example 10.1 with error norms, at $T = 0.3$, $N = 100$, and $\tau = 0.002$

x	Exact solution	Approximate solutions			
		$\lambda = 0.15$	$\lambda = 0.35$	$\lambda = 0.55$	$\lambda = 0.75$
−25	1.09	1.09	1.09	1.09	1.09
−20	1.09	1.09	1.09	1.09001	1.09003
−15	1.09	1.09	1.09	1.09	1.09003
−10	1.08998	1.08998	1.08998	1.09001	1.09001
−5	1.08761	1.08761	1.08761	1.08756	1.08764
0	1	0.999994	0.999995	1.00006	1
5	1.08761	1.08761	1.08761	1.08765	1.08763
10	1.08998	1.08998	1.08998	1.08996	1.09001
15	1.09	1.01	1.09	1.08997	1.09001
20	1.09	1.01	1.09	1.08999	1.08988
25	1.09	1.01	1.09	1.09	1.09
L_∞	⋯	5.80583×10^{-6}	5.15679×10^{-6}	7.95714×10^{-5}	1.77465×10^{-4}
L_2	⋯	6.42375×10^{-6}	1.14088×10^{-5}	3.35673×10^{-4}	2.96010×10^{-4}

Table 5: Comparison between exact and approximate solution $V(x, t)$ at x and λ, for Example 10.1 with error norms, at $T = 0.05$, $N = 100$, and $\tau = 0.002$

x	Exact solution	Approximate solutions			
		$\lambda = 0.3$	$\lambda = 0.5$	$\lambda = 0.7$	$\lambda = 0.9$
−25	6.9439×10^{-14}	7.81317×10^{-14}	9.01927×10^{-14}	7.72032×10^{-15}	2.15863×10^{-13}
−20	1.03058×10^{-11}	1.16912×10^{-9}	5.03530×10^{-9}	1.4527×10^{-9}	-2.52653×10^{-9}
−15	1.52951×10^{-9}	9.76047×10^{-9}	1.54829×10^{-9}	152807×10^{-9}	1.53077×10^{-9}
−10	2.26979×10^{-7}	2.38124×10^{-7}	2.26166×10^{-7}	2.27021×10^{-7}	2.27177×10^{-7}
−5	3.32403×10^{-5}	3.32399×10^{-5}	3.32474×10^{-5}	3.32458×10^{-5}	3.32691×10^{-5}
0	1.2500×10^{-3}	1.24953×10^{-3}	1.24730×10^{-3}	1.2473×10^{-3}	1.2512×10^{-3}
5	3.32403×10^{-5}	3.32048×10^{-5}	3.32435×10^{-5}	3.32502×10^{-5}	3.32765×10^{-5}
10	2.26979×10^{-7}	1.88161×10^{-7}	2.33882×10^{-7}	2.27044×10^{-7}	2.27225×10^{-7}
15	1.52951×10^{-9}	1.57638×10^{-8}	-2.22692×10^{-8}	2.08190×10^{-9}	1.48753×10^{-9}
20	1.03058×10^{-11}	1.18093×10^{-7}	-2.18426×10^{-7}	-1.21832×10^{-7}	-4.37435×10^{-8}
25	6.9439×10^{-14}	7.05090×10^{-14}	6.98036×10^{-14}	6.98046×10^{-14}	6.97360×10^{-14}
L_∞	⋯	4.65728×10^{-7}	1.14726×10^{-6}	2.49140×10^{-6}	1.63800×10^{-5}
L_2	⋯	6.93112×10^{-7}	1.83436×10^{-6}	2.18317×10^{-6}	4.41643×10^{-6}

$$\begin{cases} \dfrac{\partial^\lambda U(x,t)}{\partial t^\lambda} + a_1 \dfrac{\partial V(x,t)}{\partial x} + b_1 U(x,t) \dfrac{\partial U(x,t)}{\partial x} \\ \quad = Q_1(x,t), \\ \dfrac{\partial^\lambda V(x,t)}{\partial t^\lambda} + a_2 \dfrac{\partial^3 U(x,t)}{\partial x^3} + b_2 \dfrac{\partial (U(x,t)V(x,t))}{\partial x} \\ = Q_2(x,t), \end{cases} \tag{10.3}$$

$$-25 \le x \le 25, 0 \le t \le 1, 0 < \lambda < 1,$$

with ICs

$$\begin{cases} U(x,0) = \left(\dfrac{-1}{2} + \dfrac{0}{2(1 + e^{\frac{1}{2}+x})} \right) = -\dfrac{1}{2}, \\ V(x,0) = \dfrac{t}{8} \operatorname{sech}(1 + 2x) = 0, \end{cases}$$

and BCs

Table 6: Comparison between exact and approximate solution $V(x, t)$ at x and λ, for example 10.1 with error norms, at $T = 0.1$, $N = 100$, and $\tau = 0.002$

x	Exact solution	Approximate solutions			
		$\lambda = 0.2$	$\lambda = 0.4$	$\lambda = 0.6$	$\lambda = 0.8$
−25	2.77759×10^{-13}	2.75572×10^{-13}	2.67523×10^{-13}	2.48375×10^{-11}	5.72162×10^{-13}
−20	4.12231×10^{-11}	-1.66868×10^{-8}	-4.20651×10^{-9}	2.68595×10^{-8}	2.30852×10^{-8}
−15	6.11804×10^{-9}	-2.59901×10^{-8}	8.76182×10^{-8}	6.51527×10^{-9}	6.09402×10^{-9}
−10	9.07916×10^{-7}	8.59897×10^{-7}	9.75146×10^{-7}	9.6256×10^{-7}	9.08245×10^{-7}
−5	1.32961×10^{-4}	1.32901×10^{-4}	1.33185×10^{-4}	1.32995×10^{-4}	1.33007×10^{-4}
0	5.00000×10^{-3}	4.99803×10^{-3}	4.99831×10^{-3}	4.99915×10^{-3}	5.00190×10^{-3}
5	1.32961×10^{-4}	1.32976×10^{-4}	1.32528×10^{-4}	1.32986×10^{-4}	1.33047×10^{-4}
10	9.07916×10^{-7}	9.48299×10^{-7}	3.49153×10^{-7}	8.9932×10^{-7}	9.08510×10^{-7}
15	6.11804×10^{-9}	1.36481×10^{-7}	7.24536×10^{-9}	4.58022×10^{-7}	1.26859×10^{-8}
20	4.12231×10^{-11}	2.488557×10^{-7}	1.10468×10^{-6}	-4.74965×10^{-6}	-1.38330×10^{-6}
25	2.77759×10^{-13}	2.81478×10^{-13}	2.77534×10^{-13}	2.75883×10^{-13}	2.7773×10^{-13}
L_∞	⋯	1.96598×10^{-6}	2.16215×10^{-6}	1.111059×10^{-5}	2.48323×10^{-5}
L_2	⋯	2.28444×10^{-6}	4.88325×10^{-6}	1.85807×10^{-5}	2.18902×10^{-5}

$$\begin{cases} U(a,t) = \left(\dfrac{-1}{2} + \dfrac{t}{2(1+e^{\frac{-49}{2}})}\right), \\ V(a,t) = \dfrac{t}{8}\operatorname{sech}(-49), \\ U(b,t) = \left(\dfrac{-1}{2} + \dfrac{t}{2(1+e^{\frac{51}{2}})}\right), \\ V(b,t) = \dfrac{t}{8}\operatorname{sech}(51), \\ U_x(a,t) = \dfrac{-1}{2}\dfrac{e^{\frac{-49}{2}}}{(1+e^{\frac{1}{2}-25})^2}, \\ V_x(a,t) = \dfrac{-t}{4}\operatorname{sech}(-49)\tanh(-49), \\ U_x(b,t) = \dfrac{-1}{2}\dfrac{e^{\frac{51}{2}}}{(1+e^{\frac{1}{2}+25})^2}, \\ V_x(b,t) = \dfrac{-t}{4}\operatorname{sech}(51)\tanh(51). \end{cases} \tag{10.4}$$

The exact solutions are $U(x,t) = \left(\frac{-1}{2} + \frac{t}{2(1+e^{\frac{1}{2}+x})}\right)$ and $V(x,t) = \frac{t}{8}\operatorname{sech}(1+2x)$ chosen for comparison purpose between numerical solutions.

Tables 11 and 13 present the comparison between the exact and approximate solutions, along with the error norms of $U(x,t)$ at various stages of λ, with parameters $N = 100$ and $\tau = 0.002$ at different time levels $T = 0.01$ and $T = 0.03$, respectively. Tables 12 and 14 present the comparison between the exact and approximate solutions, along with the error norms of $V(x,t)$ at various stages of λ, with parameters $N = 100$ and $\tau = 0.002$ at different values of $T = 0.01$ and $T = 0.03$, respectively. Tables 15 and 16 represent the comparison between exact and approximate solutions, as well as their absolute errors, at various stages of x, with Table 15 concentrating on approximate solution $U(x,t)$, while Table 16 on approximate solution $V(x,t)$. The order of convergence is shown in Table 17 for parameters $\lambda = 0.75$ and $\tau = 0.002$. Figure 5 shows the $3D$ graphs of the exact and numerical solutions, with values of parameters $N = 80$, $\lambda = 0.7$, and $\tau = 0.002$. Figure 6 shows the $2D$ comparison between the exact and numerical solutions when the values of parameters are $N = 50$, $\lambda = 0.55$, and $\tau = 0.002$, which demonstrate the effectiveness, reliability and accuracy of the proposed method. Contour plots are presented in Figure 7, which represents the error value under the relation between x and t, with $N = 100$, $\lambda = 0.7$, and $\tau = 0.002$. The comparison is noted between exact and approximate solutions in Figure 8 at various time level $N = 100$, $\lambda = 0.7$, and $\tau = 0.002$, which demonstrate the convergence behaviour on solution by changing parameter.

Example 10.3. Take the TFCBBE with unknown exact functions, when $a_1 = a_2 = -1/2$ and $b_1 = b_2 = 2$,

$$\begin{cases} \dfrac{\partial^\lambda U(x,t)}{\partial t^\lambda} + a_1\dfrac{\partial V(x,t)}{\partial x} + b_1 U(x,t)\dfrac{\partial U(x,t)}{\partial x} \\ \quad = Q_1(x,t), \\ \dfrac{\partial^\lambda V(x,t)}{\partial t^\lambda} + a_2\dfrac{\partial^3 U(x,t)}{\partial x^3} + b_2\dfrac{\partial (U(x,t)V(x,t))}{\partial x} \\ \quad = Q_2(x,t), \end{cases} \tag{10.5}$$

$$-25 \le x \le 25,\ 0 \le t \le 1,\ 0 < \lambda < 1.$$

Table 7: Comparison between exact and approximate solution $V(x,t)$ at x and λ, for example 10.1 with error norms, at $T = 0.3$, $N = 100$, and $\tau = 0.002$

x	Exact solution	Approximate solutions			
		$\lambda = 0.15$	$\lambda = 0.35$	$\lambda = 0.55$	$\lambda = 0.75$
−25	2.49983×10^{-12}	2.50520×10^{-12}	2.67523×10^{-13}	2.48375×10^{-11}	5.72162×10^{-13}
−20	3.71008×10^{-10}	-2.23915×10^{-7}	-4.20651×10^{-9}	2.68595×10^{-8}	2.30852×10^{-8}
−15	5.50624×10^{-8}	-1.87616×10^{-7}	8.76182×10^{-8}	6.51527×10^{-9}	6.09402×10^{-9}
−10	8.17125×10^{-6}	7.93872×10^{-6}	9.75146×10^{-7}	9.6256×10^{-7}	9.08245×10^{-7}
−5	1.19665×10^{-3}	1.19647×10^{-3}	1.33185×10^{-4}	1.32995×10^{-4}	1.33007×10^{-4}
0	4.50000×10^{-2}	4.49825×10^{-2}	4.99831×10^{-3}	4.99915×10^{-3}	5.00190×10^{-3}
5	1.19665×10^{-3}	1.19707×10^{-3}	1.32528×10^{-4}	1.32986×10^{-4}	1.33047×10^{-4}
10	8.17125×10^{-6}	8.75482×10^{-6}	3.49153×10^{-7}	8.9932×10^{-7}	9.08510×10^{-7}
15	5.50624×10^{-8}	1.05676×10^{-6}	7.24536×10^{-9}	4.58022×10^{-7}	1.26859×10^{-8}
20	3.71008×10^{-10}	1.50328×10^{-6}	1.10468×10^{-6}	-4.74965×10^{-6}	-1.38330×10^{-6}
25	2.49983×10^{-12}	2.50222×10^{-12}	2.77534×10^{-13}	2.75883×10^{-13}	2.7773×10^{-13}
L_∞	⋯	1.74828×10^{-5}	1.91166×10^{-5}	2.03757×10^{-4}	6.29592×10^{-4}
L_2	⋯	1.95213×10^{-5}	3.89036×10^{-5}	9.44123×10^{-4}	1.12051×10^{-3}

Table 8: Absolute errors of approximate solution $U(x, t)$, for example 10.1, when $T = 0.01$, $\tau = 0.01$, and $N = 100$

x	Exact solution	Approximate solutions		Absolute errors	
		$\lambda = 0.35$	$\lambda = 0.55$	$\lambda = 0.35$	$\lambda = 0.55$
−25	1.001	1.001	1.001	1.99840×10^{-15}	5.70655×10^{-14}
−20	1.001	1.001	1.001	1.76247×10^{-8}	6.78361×10^{-8}
−15	1.001	1.001	1.001	1.76096×10^{-8}	6.78581×10^{-8}
−10	1.001	1.001	1.001	1.75980×10^{-8}	6.78474×10^{-8}
−5	1.001	1.001	1.001	1.72850×10^{-8}	6.62821×10^{-8}
0	1	1	1	1.38537×10^{-10}	7.69183×10^{-10}
5	1.0001	1.0001	1.001	1.66250×10^{-8}	6.57614×10^{-8}
10	1.0001	1.0001	1.001	1.81281×10^{-8}	6.78437×10^{-8}
15	1.0001	1.0001	1.001	2.01267×10^{-8}	6.78633×10^{-8}
20	1.0001	1.0001	1.001	1.24716×10^{-9}	6.7998×10^{-8}
25	1.0001	1.0001	1.001	2.66454×10^{-15}	4.10783×10^{-14}

Table 9: Absolute errors of approximate solution $V(x, t)$, for example 10.1, when $T = 0.01$, $\tau = 0.01$, and $N = 100$

x	Exact solution	Approximate solutions		Absolute errors	
		$\lambda = 0.35$	$\lambda = 0.55$	$\lambda = 0.35$	$\lambda = 0.55$
−25	2.77759×10^{-15}	1.33013×10^{-14}	7.67832×10^{-14}	1.05237×10^{-14}	7.40056×10^{-14}
−20	4.12231×10^{-13}	-6.20959×10^{-11}	-1.79339×10^{-11}	6.25081×10^{-11}	1.83461×10^{-11}
−15	6.11804×10^{-11}	5.60952×10^{-11}	6.11649×10^{-11}	5.08523×10^{-12}	1.55260×10^{-14}
−10	9.07916×10^{-9}	9.07363×10^{-9}	9.08438×10^{-9}	5.53505×10^{-12}	5.22331×10^{-12}
−5	1.32961×10^{-6}	1.32992×10^{-6}	1.33036×10^{-6}	3.08799×10^{-10}	7.50350×10^{-10}
0	5.00000×10^{-5}	4.99957×10^{-5}	5.00318×10^{-5}	4.27955×10^{-9}	3.18371×10^{-8}
5	1.32961×10^{-6}	1.32951×10^{-6}	1.33071×10^{-6}	1.05238×10^{-10}	1.10208×10^{-9}
10	9.07916×10^{-9}	1.53254×10^{-8}	9.08667×10^{-9}	6.24626×10^{-9}	7.50843×10^{-12}
15	6.11804×10^{-11}	-2.41473×10^{-8}	7.88437×10^{-11}	2.42084×10^{-8}	1.76633×10^{-11}
20	4.12231×10^{-13}	-1.12954×10^{-8}	-6.71191×10^{-9}	1.12958×10^{-8}	6.71233×10^{-9}
25	2.77759×10^{-15}	2.53736×10^{-15}	1.84033×10^{-15}	2.40229×10^{-16}	9.37258×10^{-16}

Table 10: Order of convergence for example 10.1, with $\lambda = 0.3$ and $\tau = 0.002$

N	$\|L\|_\infty$	Order	CPU	$\|L\|_\infty$	Order	CPU
	$U(x, t)$			$V(x, t)$		
40	7.63248×10^{-8}	⋯	9.829 s	6.61393×10^{-8}	⋯	9.829 s
80	1.79784×10^{-8}	2.08589	17.656 s	1.74396×10^{-8}	1.92314	17.656 s
160	4.80419×10^{-9}	1.90390	46.891 s	4.17423×10^{-9}	2.06278	46.891 s
320	1.21730×10^{-9}	1.98061	113.342 s	1.03184×10^{-9}	2.01629	113.342 s

Table 18 represents the approximate solutions at various stages of x for $U(x, t)$ and $V(x, t)$. Figure 9 shows the 3D graphs of approximate solutions, with values of parameters $N = 50$, $\lambda = 0.55$, and $\tau = 0.002$ for $U(x, t)$ and $V(x, t)$. Figure 10 shows the 2D approximate solutions when the values of parameters are $N = 50$, $\lambda = 0.55$, and $\tau = 0.002$ for $U(x, t)$ and $V(x, t)$. Figure 11 shows the approximate solutions at different values of λ and fixing $N = 100$, and $\tau = 0.002$.

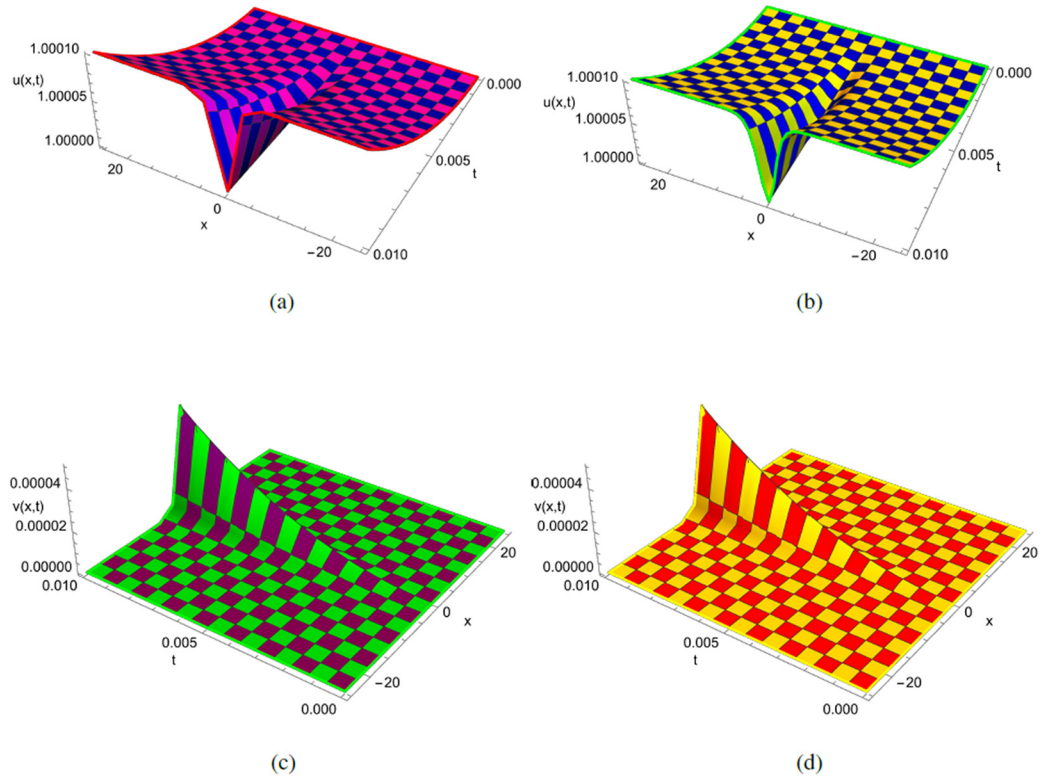

Figure 1: Space-time graph comparison between exact and approximate solutions, for example 10.1. (a) Exact solution $U(x, t)$, (b) approximate solution $U(x, t)$, (c) exact solution $V(x, t)$, and (d) approximate solution $V(x, t)$.

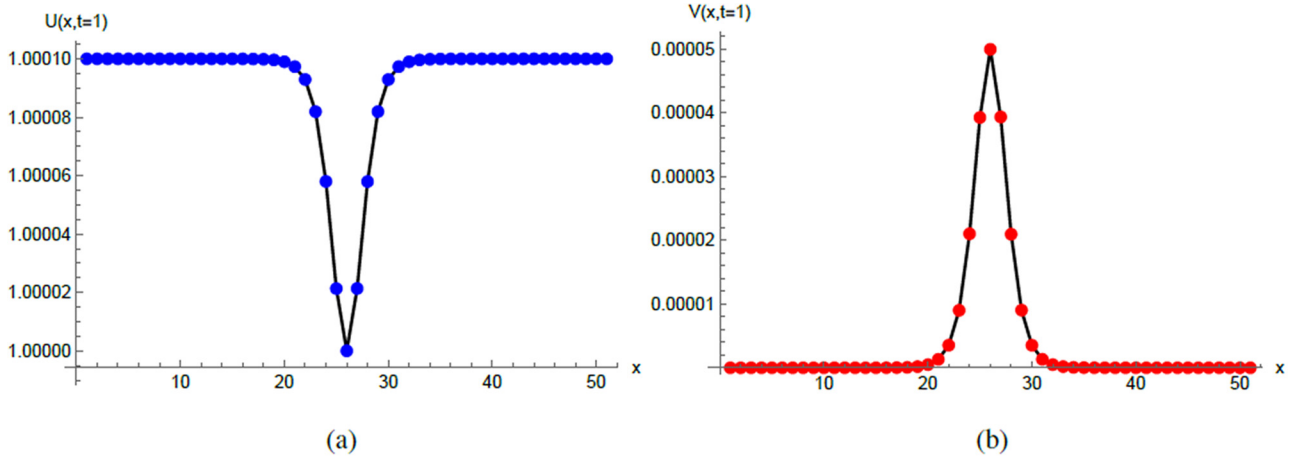

Figure 2: Comparison between 2D exact and approximate solutions, for example 10.1. (a) 2D exact and approximate solutions $U(x, t)$ and (b) 2D exact and approxi solutions $V(x, t)$.

11 Conclusion

This study provided a new way to use QBS functions to solve a time–fractional version of the CBBE model. The model based on describing wave transmission in shallow water and other physical phenomena in fields like fluid mechanics and plasma waves. In addition, it helped to understanding their solutions provided insights into non-linear wave behaviours, such as bell-shaped and kink-shaped waves in fluid dynamics and optics. Moreover, it

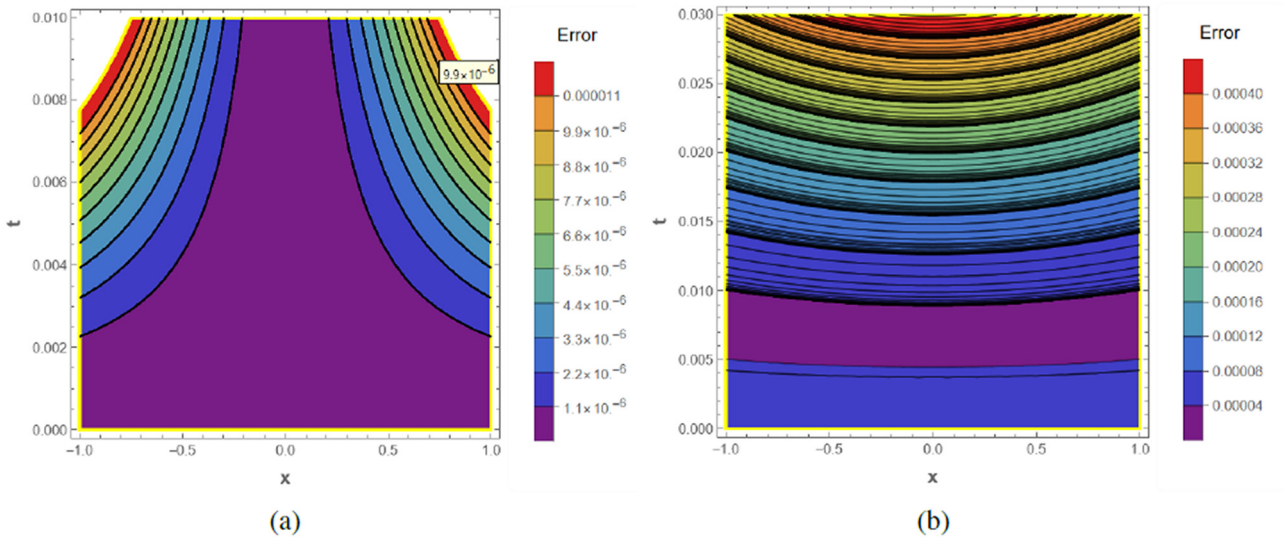

Figure 3: Contour plot for example 10.1. (a) Error analysis $U(x, t)$ and (b) error analysis of $V(x, t)$.

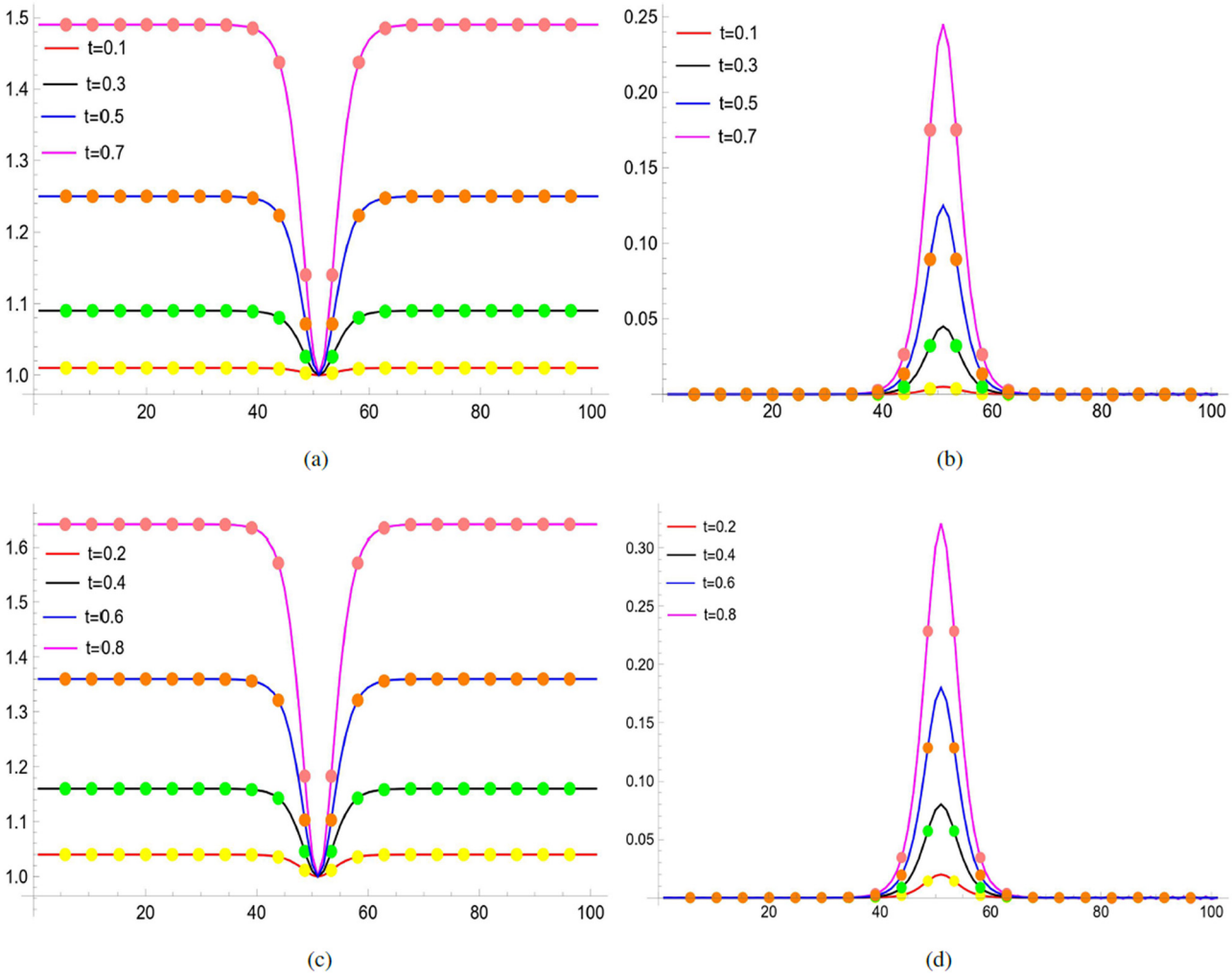

Figure 4: Comparison between exact and approximate solutions at various time levels, for example 10.1. (a) For $U(x, t)$, (b) for $V(x, t)$, (c) for $U(x, t)$, (d) for $V(x, t)$.

Table 11: Comparison between exact and approximate solution of $U(x, t)$ at x and λ, for example 10.2 with error norms, at $T = 0.01$, $N = 100$, and $\tau = 0.002$

x	Exact solution	Approximate solutions			
		$\lambda = 0.3$	$\lambda = 0.5$	$\lambda = 0.7$	$\lambda = 0.9$
−25	−0.495	−0.495	−0.495	−0.495	−0.495
−20	−0.495	−0.494985	−0.49501	−0.49501	−0.49501
−15	−0.495	−0.494982	−0.49501	−0.49501	−0.49501
−10	−0.495	−0.494999	−0.49501	−0.49501	−0.49501
−5	−0.495055	−0.495078	−0.495065	−0.495065	−0.495065
0	−0.498112	−0.498203	−0.498116	−0.498116	−0.498116
5	−0.49998	−0.499942	−0.49998	−0.49998	−0.49998
10	−0.5	−0.499997	−0.5	−0.5	−0.5
15	−0.5	−0.500005	−0.5	−0.5	−0.5
20	−0.5	−0.499999	−0.5	−0.5	−0.5
25	−0.5	−0.5	−0.5	−0.5	−0.5
L_∞	⋯	9.80707×10^{-5}	2.02848×10^{-5}	1.69836×10^{-5}	1.59361×10^{-5}
L_2	⋯	2.44472×10^{-4}	4.97967×10^{-5}	483436×10^{-5}	4.7895×10^{-5}

Table 12: Comparison between exact and approximate solution of $V(x, t)$ at x and λ, for example 10.1 with error norms, at $T = 0.01$, $N = 100$, and $\tau = 0.002$

x	Exact solution	Approximate solutions			
		$\lambda = 0.3$	$\lambda = 0.5$	$\lambda = 0.7$	$\lambda = 0.9$
−25	1.31072×10^{-24}	4.15862×10^{-15}	-3.91801×10^{-14}	2.01169×10^{-13}	1.3826×10^{-13}
−20	2.88706×10^{-20}	5.15983×10^{-5}	-6.38002×10^{-7}	-1.16338×10^{-7}	-2.5133×10^{-8}
−15	6.35916×10^{-16}	3.16867×10^{-5}	5.45180×10^{-9}	2.57366×10^{-12}	-1.5991×10^{-11}
−10	1.40070×10^{-11}	2.29476×10^{-4}	9.75146×10^{-7}	3.18296×10^{-11}	2.07311×10^{-11}
−5	3.08525×10^{-7}	3.70708×10^{-4}	2.82478×10^{-7}	3.13345×10^{-7}	3.09519×10^{-7}
0	8.10068×10^{-4}	649279×10^{-4}	8.03862×10^{-4}	8.0758×10^{-4}	8.08229×10^{-4}
5	4.17543×10^{-8}	1.74435×10^{-4}	8.15252×10^{-8}	4.40967×10^{-8}	4.2046×10^{-8}
10	1.89564×10^{-12}	8.69702×10^{-5}	-1.78631×10^{-10}	8.69448×10^{-12}	4.27815×10^{-12}
15	8.60619×10^{-17}	-1.37061×10^{-5}	8.39288×10^{-13}	4.07394×10^{-14}	1.69271×10^{-14}
20	3.90721×10^{-21}	-8.7289×10^{-6}	-1.21386×10^{-14}	-1.11335×10^{-15}	4.47313×10^{-15}
25	1.77387×10^{-25}	-5.06571×10^{-16}	2.04785×10^{-16}	-1.09588×10^{-16}	-3.97781×10^{-16}
L_∞	⋯	4.66635×10^{-4}	3.33530×10^{-5}	1.12099×10^{-5}	7.50260×10^{-6}
L_2	⋯	1.12198×10^{-3}	3.12980×10^{-5}	8.99922×10^{-6}	6.04422×10^{-6}

Table 13: Comparison between exact and approximate solution of $U(x, t)$ at x and λ, for example 10.2 with error norms, at $T = 0.03$, $N = 100$, and $\tau = 0.002$

x	Exact solution	Approximate solutions			
		$\lambda = 0.25$	$\lambda = 0.45$	$\lambda = 0.65$	$\lambda = 0.85$
−25	−0.485	−0.485	−0.485	−0.485	−0.485
−20	−0.485	−0.484998	−0.485066	−0.48503	−0.485029
−15	−0.485	−0.484995	−0.485018	−0.48503	−0.485029
−10	−0.485001	−0.485013	−0.485031	−0.485031	−0.48503
−5	−0.485165	−0.485202	−0.485195	−0.485194	−0.48503
0	−0.494337	−0.494367	−0.494334	−0.494349	−0.494349
5	−0.499939	−0.499955	−0.499939	−0.499939	−0.499939
10	−0.5	−0.499994	−0.5	−0.5	−0.5
15	−0.5	−0.499982	−0.5	−0.5	−0.5
20	−0.5	−0.499992	−0.5	−0.5	−0.5
25	−0.5	−0.5	−0.5	−0.5	−0.5
L_∞	⋯	5.80583×10^{-6}	1.75136×10^{-4}	6.01763×10^{-5}	5.15177×10^{-5}
L_2	⋯	6.42375×10^{-6}	2.62023×10^{-4}	1.47854×10^{-4}	1.4405×10^{-4}

Table 14: Comparison between exact and approximate solution of $V(x, t)$ at x and λ, for example 10.2 with error norms, at $T = 0.03$, $N = 100$, and $\tau = 0.002$

x	Exact solution	Approximate solutions			
		$\lambda = 0.15$	$\lambda = 0.35$	$\lambda = 0.55$	$\lambda = 0.75$
−25	3.93216×10^{-24}	2.42861×10^{-16}	4.30016×10^{-15}	-2.43008×10^{-13}	-2.8619×10^{-13}
−20	8.66117×10^{-20}	1.3338×10^{-4}	-458796×10^{-4}	-1.58780×10^{-6}	-4.39797×10^{-7}
−15	1.90775×10^{-15}	-1.43843×10^{-4}	8.89565×10^{-6}	1.28768×10^{-8}	6.09402×10^{-9}
−10	4.2021×10^{-11}	-1.19366×10^{-4}	1.83923×10^{-6}	2.06518×10^{-10}	-3.07743×10^{-10}
−5	9.25574×10^{-7}	1.24296×10^{-4}	1.33185×10^{-6}	8.96957×10^{-7}	9.43235×10^{-7}
0	2.43020×10^{-3}	2.40235×10^{-3}	2.43679×10^{-3}	2.41439×10^{-3}	2.42246×10^{-3}
5	1.25263×10^{-7}	6.87115×10^{-5}	1.70851×10^{-5}	2.00331×10^{-7}	1.33549×10^{-7}
10	5.68692×10^{-12}	9.2443×10^{-4}	-5.31934×10^{-7}	-1.50672×10^{-10}	3.03963×10^{-11}
15	2.58186×10^{-16}	1.42914×10^{-5}	-1.22619×10^{-8}	4.19551×10^{-13}	1.37607×10^{-13}
20	1.17216×10^{-20}	-6.39416×10^{-5}	7.42182×10^{-10}	-1.1474×10^{-14}	1.16415×10^{-14}
25	5.32161×10^{-25}	-4.78926×10^{-16}	-1.64338×10^{-16}	4.93712×10^{-17}	-1.40068×10^{-16}
L_∞	⋯	2.43737×10^{-4}	5.50774×10^{-4}	8.78161×10^{-5}	3.70859×10^{-5}
L_2	⋯	6.95266×10^{-4}	1.01278×10^{-5}	8.06507×10^{-5}	302112×10^{-5}

Table 15: Absolute errors of $U(x, t)$ for example 10.2, when $T = 0.01$, $\tau = 0.01$, and $N = 100$

x	Exact solution	Approximate solutions		Absolute errors	
		$\lambda = 0.75$	$\lambda = 0.95$	$\lambda = 0.75$	$\lambda = 0.95$
−25	−0.495	−0.495	−0.495	4.87332×10^{-13}	6.86423×10^{-14}
−20	−0.495	−0.49501	−0.49501	9.82669×10^{-6}	9.85125×10^{-8}
−15	−0.495	−0.49501	−0.49501	9.82836×10^{-6}	9.85576×10^{-6}
−10	−0.495	−0.49501	−0.49501	9.82760×10^{-6}	9.85501×10^{-6}
−5	−0.495055	−0.495065	−0.495065	9.71667×10^{-6}	9.74600×10^{-6}
0	−0.498112	−0.498116	−0.498116	3.87346×10^{-6}	3.77554×10^{-6}
5	−0.49998	−0.49998	−0.49998	3.88119×10^{-8}	3.96451×10^{-8}
10	−0.5	−0.5	2.68014	2.61624×10^{-10}	2.68014×10^{-10}
15	−0.5	−0.5	−0.5	1.73955×10^{-12}	1.80456×10^{-12}
20	−0.5	−0.5	−0.5	7.10543×10^{-15}	1.92624×10^{-14}
25	−0.5	−0.5	−0.5	7.53286×10^{-14}	2.29317×10^{-13}

Table 16: Absolute errors of $V(x, t)$ for example 10.2 at $T = 0.01$, $\tau = 0.01$, and $N = 100$

x	Exact solution	Approximate solutions		Absolute errors	
		$\lambda = 0.75$	$\lambda = 0.95$	$\lambda = 0.75$	$\lambda = 0.95$
−25	1.31072×10^{-24}	1.53111×10^{-13}	-2.83178×10^{-12}	1.53111×10^{-13}	2.83178×10^{-12}
−20	2.88706×10^{-20}	-7.81670×10^{-8}	-1.74722×10^{-8}	7.81670×10^{-8}	1.74722×10^{-8}
−15	6.35916×10^{-16}	-2.88217×10^{-11}	-1.13142×10^{-11}	2.88223×10^{-11}	1.13148×10^{-11}
−10	1.40070×10^{-11}	2.81635×10^{-11}	0.92180×10^{-11}	1.41565×10^{-11}	55.21104×10^{-12}
−5	3.08525×10^{-7}	3.12071×10^{-7}	3.09086×10^{-7}	3.54663×10^{-9}	5.61068×10^{-10}
0	8.10068×10^{-4}	8.07838×10^{-4}	8.08283×10^{-4}	2.22965×10^{-6}	1.78443×10^{-6}
5	4.17543×10^{-8}	4.30710×10^{-8}	4.19361×10^{-8}	1.31680×10^{-9}	1.81843×10^{-10}
10	1.89564×10^{-12}	7.12717×10^{-12}	3.73727×10^{-12}	5.23153×10^{-12}	1.84163×10^{-12}
15	8.60619×10^{-17}	3.48272×10^{-14}	3.74397×10^{-14}	3.47411×10^{-14}	3.65177×10^{-14}
20	3.90721×10^{-21}	-3.08899×10^{-15}	3.03725×10^{-14}	3.08899×10^{-15}	3.03725×10^{-14}
25	1.77387×10^{-25}	-3.76144×10^{-16}	5.59587×10^{-17}	3.76144×10^{-16}	5.59587×10^{-17}

Table 17: Order of convergence for example 10.2 when $\lambda = 0.3$ and $\tau = 0.002$

N	$\|L\|_\infty$	Order	CPU	$\|L\|_\infty$	Order	CUP
	$U(x,t)$			$V(x,t)$		
40	1.58885×10^{-5}	⋯	13.984 s	2.04443×10^{-4}	⋯	13.984 s
80	4.23290×10^{-6}	1.90827	23.451 s	4.88503×10^{-5}	2.06526	23.451 s
160	1.07637×10^{-6}	1.90390	53.969 s	1.24173×10^{-5}	1.97602	53.969 s
320	2.53249×10^{-7}	2.08755	120.786 s	2.93454×10^{-6}	2.08115	120.796 s

can be applied to simulate real-world phenomena such as tsunami propagation, sediment transport, and wave interactions in optical fibres under some limitations like BCs and parameter tuning, which depend on scenarios. The approach combined the QBS functions with the Crank–Nicholson scheme and θ-weighted method, delivering a smooth, accurate solution with C^4 continuity at joints. The Caputo fractional derivative employed to handle the fractional aspect of the model. This is the first application of the proposed method to this equation, highlighting its novelty in achieving enhanced precision and stability for fractional–order models. To assess how effective the suggested numerical algorithm is,

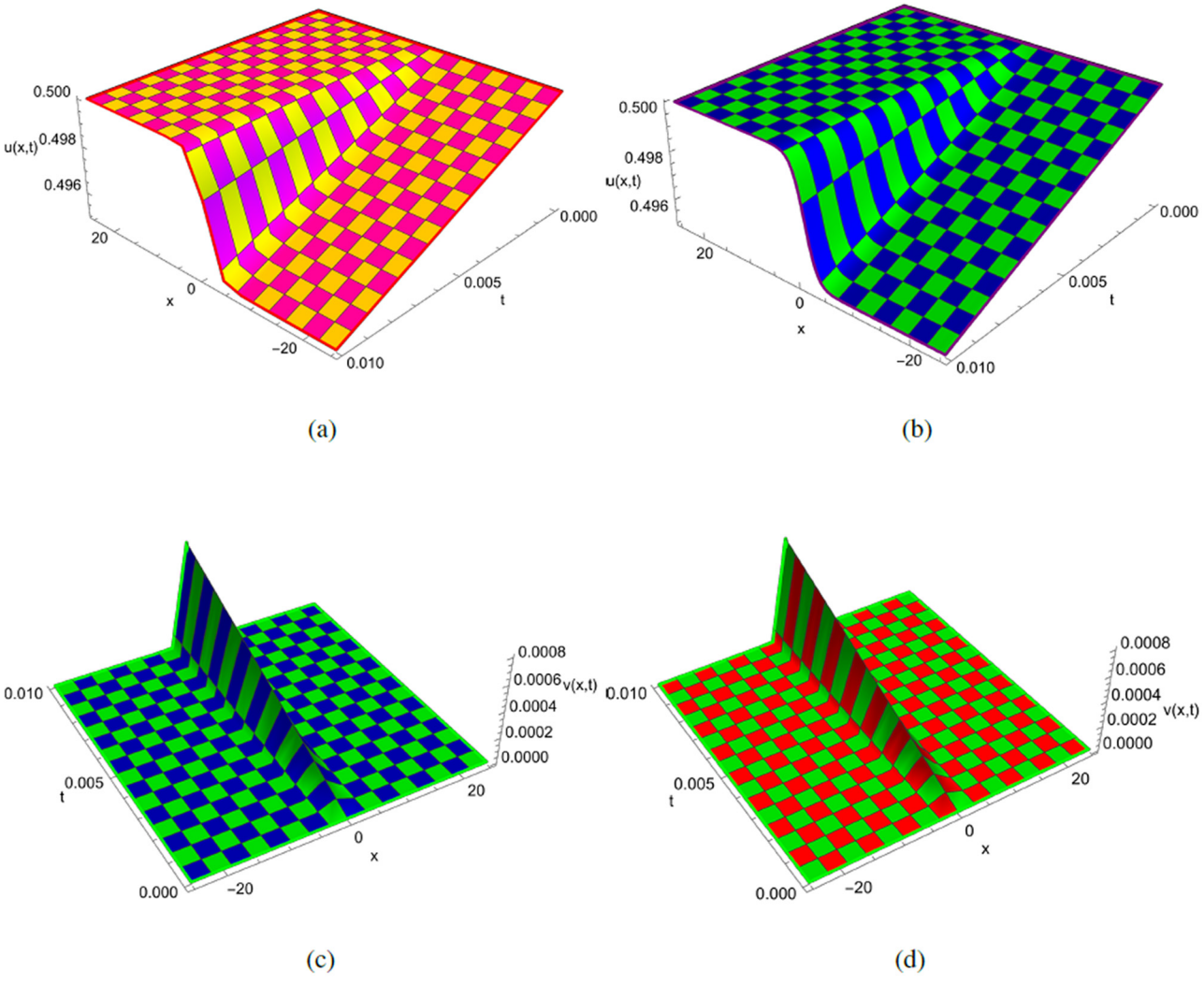

Figure 5: 3D graph comparison between exact and approximate solutions, for example 10.2. (a) Exact solution $U(x,t)$, (b) approximate solution $U(x,t)$, (c) exact solution $V(x,t)$, and (d) approximate solution $V(x,t)$.

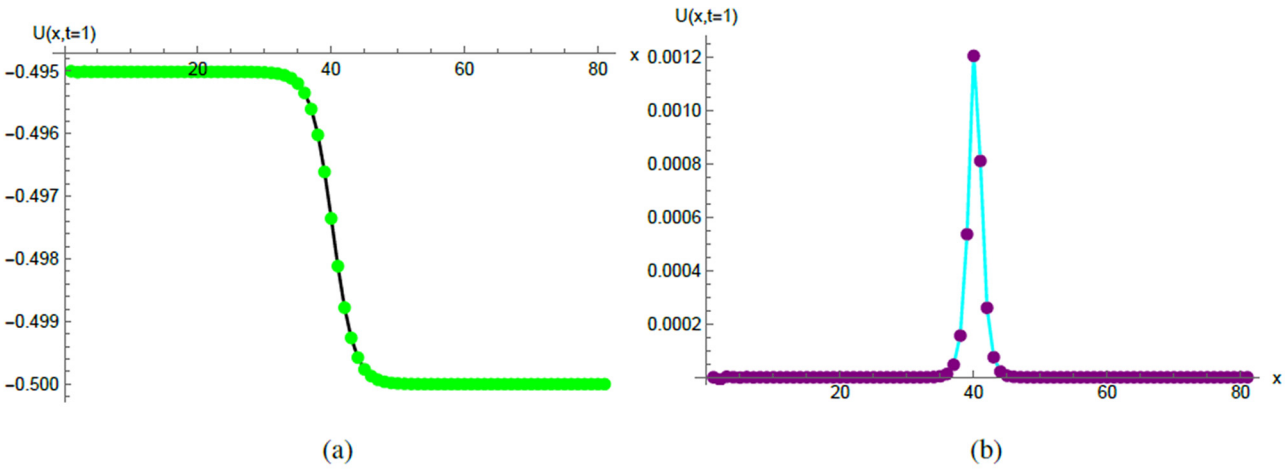

Figure 6: 2D graph comparison between exact and approximate solutions, for example 10.2. (a) 2D exact and approximate solutions $U(x, t)$ and (b) 2D exact and approximate solutions $V(x, t)$.

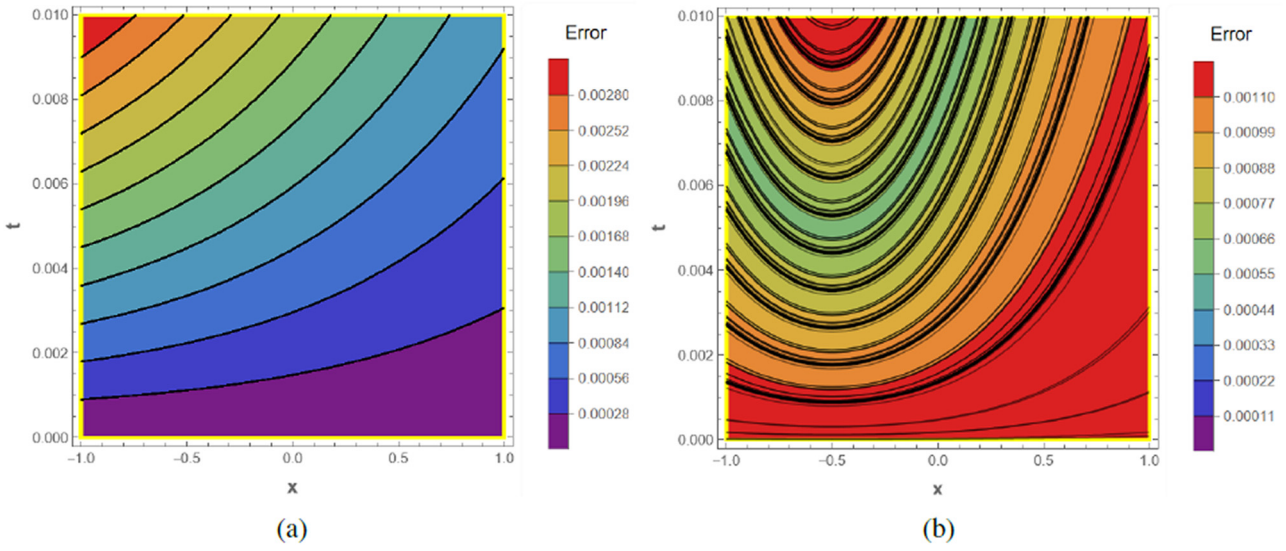

Figure 7: Contour plot, for example 10.2. (a) Error analysis $U(x, t)$ and (b) error analysis of $V(x, t)$.

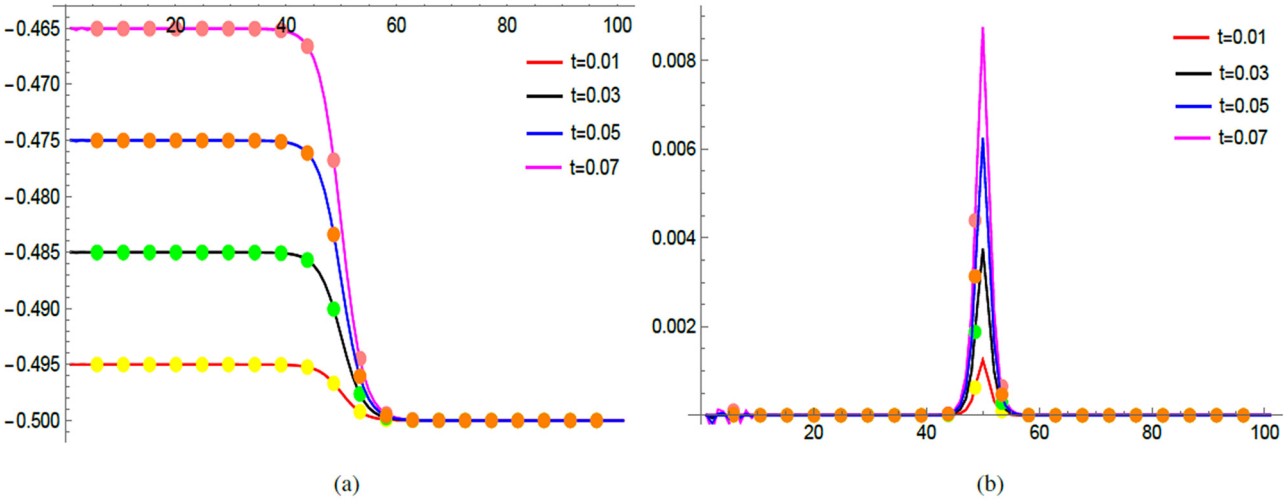

Figure 8: 2D graph comparison between exact and approximate solutions, for example 10.2. (a) For $U(x, t)$ and (b) for $V(x, t)$.

Table 18: Approximate solution for example 10.3 at $T = 0.01$, $\tau = 0.002$, and $N = 80$

	For $U(x, t)$			For $V(x, t)$		
x	$\lambda = 0.375$	$\lambda = 0.575$	$\lambda = 0.775$	$\lambda = 0.375$	$\lambda = 0.575$	$\lambda = 0.775$
−25	0.5001	0.5001	0.5001	8.65349×10^{-15}	-9.15430×10^{-14}	-2.65199×10^{-13}
−20	0.5001	0.5001	0.5001	2.34154×10^{-11}	1.76253×10^{-11}	1.96344×10^{-10}
−15	0.5001	0.5001	0.5001	3.12554×10^{-11}	3.04940×10^{-11}	3.08183×10^{-11}
−10	0.5001	0.5001	0.5001	4.52402×10^{-9}	4.54006×10^{-9}	4.54131×10^{-9}
−5	0.500097	0.500097	0.500097	6.64732×10^{-7}	6.64853×10^{-7}	6.65050×10^{-7}
0	0.5	0.5	0.5	2.49678×10^{-5}	2.49998×10^{-5}	2.50095×10^{-5}
5	0.500097	0.500097	0.500097	6.64640×10^{-7}	6.4891×10^{-7}	6.65081×10^{-7}
10	0.5001	0.5001	0.5001	4.53646×10^{-9}	4.53982×10^{-9}	4.54137×10^{-9}
15	0.5001	0.5001	0.5001	1.01887×10^{-10}	2.99043×10^{-11}	2.07756×10^{-11}
20	0.5001	0.5001	0.5001	-1.35719×10^{-9}	-3.01356×10^{-10}	-1.87493×10^{-10}
25	0.5001	0.5001	0.5001	1.42570×10^{-15}	1.32021×10^{-15}	1.45449×10^{-15}

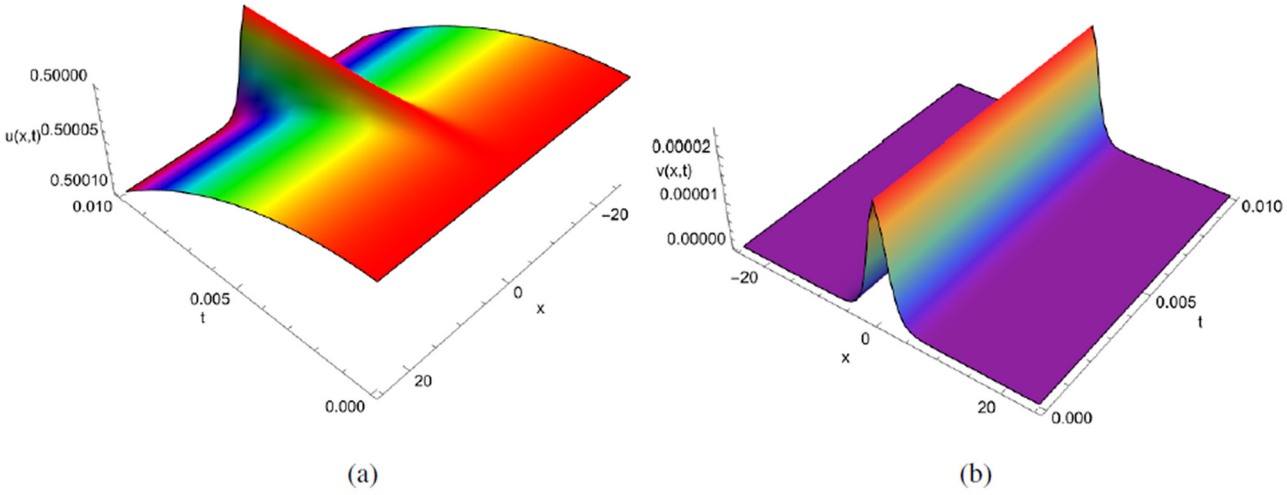

Figure 9: 3D graph of approximate solutions, for example 10.3. (a) Approximate solution $U(x, t)$ and (b) approximate solution $V(x, t)$.

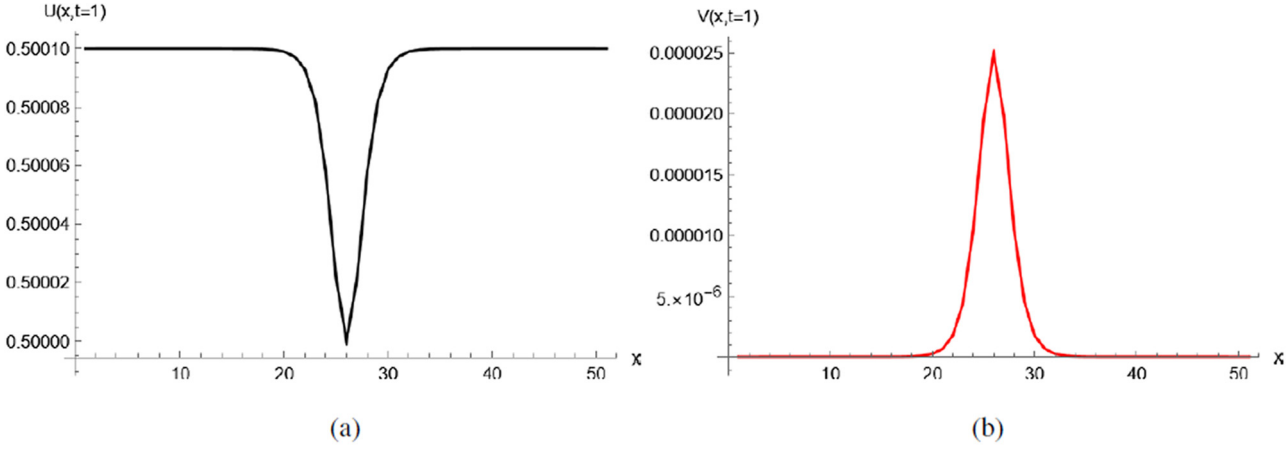

Figure 10: 2D graph of approximate solutions, for example 10.3. (a) 2D exact and approximate solutions $U(x, t)$ and (b) 2D exact and approximate solutions $V(x, t)$.

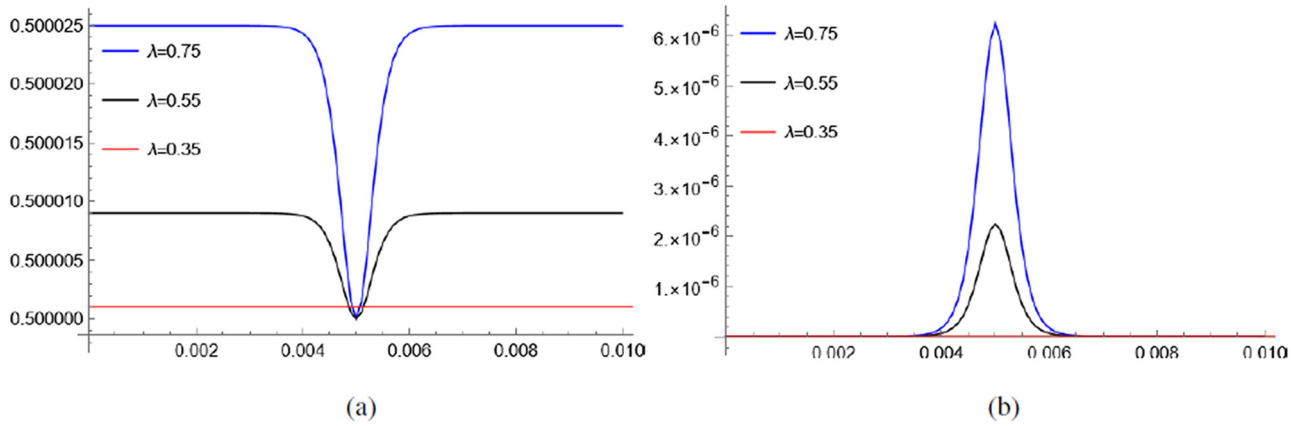

Figure 11: Approximate solution at different value of λ, for example 10.3. (a) Error analysis $U(x, t)$ and (b) error analysis of $V(x, t)$.

we have solved two new numerical test problems that have never been considered previously. The numerical algorithm represented the unconditionally stability of the proposed scheme. The correctness and usefulness of the technique have been demonstrated by the findings displayed in the tables and figures. The differences between exact and approximate values have been compared, and the errors between them have been identified. The numerical findings have been obtained with help of Mathematica 13.2 and concluded that the proposed approach provided a more satisfactory results. Future scope of the suggested technique will extend it for solving multi-variate fractional models, which help us to investigate complex wave dynamics in multi-dimensional shallow water systems. In other words, the suggested approach is extensible and can be used to solve more nonlinear partial differential equations that come up in mathematical physics.

11.1 Key advantages of using the QBS collocation method

The QBS collocation method is a potent tool for solving fractional and classical differential equations because it has a number of benefits. The great precision, stability, and C^4 smoothness of the QBS collocation method make it beneficial. It is particularly useful for issues that call for the depiction of complex geometries, smooth solutions, or higher-order derivatives. It is a flexible and dependable approach for sophisticated numerical simulations and analyzis because of these benefits. It provides a numerical solution in piecewise polynomial form having C^4 continuity at the joint points of the equally spaced domain. It also provides a numerical solution at each point of the domain.

11.2 Limitations of the QBS collocation method

High accuracy and smoothness are provided by the QBS collocation method, but like any method, it has certain limitations: compared to cubic or quartic B-splines, the functions involving more terms result in more complex calculations, higher memory usage, more complicated implementation, and sensitivity to problem setup in terms of collocation points and knots. It works best in applications that demand high accuracy and have a smooth problem domain and solution. However, other approaches might be more useful for irregular domains, large-scale calculations, or non-smooth situations.

Acknowledgments: This research was supported by the Science and Technology Research Project of Jiangxi Provincial Department of Education (Grant No. GJJ2201802) and Jiangxi Province Key Laboratory of Applied Optical Technology (2024SSY03051). The authors extend their appreciation to Taif University, Saudi Arabia, for supporting this work through project number (TU-DSPP-2024-47).

Funding information: This research was funded by Taif University, Saudi Arabia, Project No. (TU-DSPP-2024-47).

Author contributions: XW: validation, visualization, methodology. UG: methodology, writing – original draft, writing – review, and editing. MA: supervision, visualization, methodology, writing – original draft, writing – review, and editing. FAA: validation, visualization, software, writing – original draft. YSH: validation, formal analyzis, visualization, writing – original draft. All authors have accepted responsibility for the entire content of this manuscript and approved its submission.

Conflict of interest: The authors state no conflict of interest.

Data availability statement: All data generated or analysed during this study are included in this published article.

References

[1] Kilbas AA, Srivastava HM, Trujillo JJ. Theory and applications of fractional differential equations. Vol. 204. New York: Elsevier; 2006.

[2] Podlubny I. Fractional Differential Equations. New York: Academic Press; 1999.

[3] Sabatier J, Agrawal OP, Machado JAT. Advances in fractional calculus: Theoretical developments and applications in physics and engineering. Vol. 4, No. 9. Dordrecht: Springer; 2007.

[4] Miller KS, Ross B. An introduction to the fractional calculus and fractional differential equations. New York: John Wiley & Sons, Inc.; 1993.

[5] Vinagre BM, Podlubny I, Hernandez A, Feliu V. Some approximations of fractional-order operators used in control theory and applications. Fract Calculus Appl Anal. 2000;3(3):231–48.

[6] Oldham K, Spanier J. The fractional calculus theory and applications of differentiation and integration to arbitrary order. New York: Elsevier; 1974.

[7] Samko SG. Fractional integrals and derivatives. Theory and Applications. 1993.

[8] Tchier F, Yusuf A, Aliyu AI, Baleanu D. Time fractional third-order variant Boussinesq system: symmetry analyzis, explicit solutions, conservation laws and numerical approximations. Europ Phys J Plus. 2018;133(6):240.

[9] Yang XJ, Baleanu D, Srivastava HM. Local fractional integral transforms and their applications. New York: Academic Press; 2015.

[10] Zhang J, Wu Y, Li X. Quasi-periodic solution of the (2+1)-dimensional Boussinesq-Burgers soliton equation. Phys A Stat Mech Appl. 2003;319:213–32.

[11] Zhang L, Zhang L-F, Li C-Y. Some new exact solutions of Jacobian elliptic function about the generalized Boussinesq equation and Boussinesq-Burgers equation. Chinese Phys B. 2008;17(2):403.

[12] Rady AA, Khalfallah M. On soliton solutions for Boussinesq-Burgers equations. Commun Nonlinear Sci Numer Simul. 2010;15(4):886–94.

[13] Chen A, Li X. Darboux transformation and soliton solutions for Boussinesq-Burgers equation. Chaos Solitons Fractals. 2006;27(1):43–9.

[14] Gupta AK, Ray SS. Comparison between homotopy perturbation method and optimal homotopy asymptotic method for the soliton solutions of Boussinesq-Burger equations. Comput Fluids. 2014;103:34–41.

[15] Wang KJ, Wang GD, Zhu HW. A new perspective on the study of the fractal coupled Boussinesq-Burger equation in shallow water. Fractals. 2021;29(5):2150122.

[16] Kumar S, Kumar A, Baleanu D. Two analytical methods for time-fractional nonlinear coupled Boussinesq-Burger's equations arise in propagation of shallow water waves. Nonlinear Dyn. 2016;85:699–715.

[17] Khater MM, Kumar D. New exact solutions for the time fractional coupled Boussinesq-Burger equation and approximate long water wave equation in shallow water. J Ocean Eng Sci. 2017;2(3):223–8.

[18] Shi D, Zhang Y, Liu W, Liu J. Some exact solutions and conservation laws of the coupled time-fractional Boussinesq-Burgers system. Symmetry. 2019;11(1):77.

[19] Ravi LK, Ray SS, Sahoo S. New exact solutions of coupled Boussinesq-Burgers equations by exp-function method. J Ocean Eng Sci. 2017;2(1):34–46.

[20] Ali KK, Yilmazer R, Bulut H. Analytical solutions to the coupled Boussinesq-Burgers equations via Sine-Gordon expansion method. In 4th International Conference on Computational Mathematics and Engineering Sciences (CMES-2019). Springer International Publishing; Vol. 4. 2020. p. 233–40.

[21] Heydari MH, Avazzadeh Z. New formulation of the orthonormal Bernoulli polynomials for solving the variable-order time fractional coupled Boussinesq-Burger's equations. Eng Comput. 2021;37:3509–17.

[22] Zarin R, Khaliq H, Khan A, Ahmed I, Humphries UW. A numerical study based on haar wavelet collocation methods of fractional-order antidotal computer virus model. Symmetry. 2023;15(3):621.

[23] Jitsinchayakul S, Zarin R, Khan A, Yusuf A, Zaman G., Humphries UW, et al. Fractional modelling of COVID-19 epidemic model with harmonic mean type incidence rate. Open Phys. 2021;19(1):693–709.

[24] Chu YM, Zarin R, Khan A, Murtaza S. A vigorous study of fractional-order mathematical model for SARS-CoV-2 epidemic with Mittag-Leffler kernel. Alex Eng J. 2023;71:565–79.

[25] Zarin R. Numerical study of a nonlinear COVID-19 pandemic model by finite difference and meshless methods. Partial Differ Equ Appl Math. 2022;6:100460.

[26] Zhang Z, Wang F. The space-time semi-analytical meshless methods for coupled Burgers' equations. Wuhan Univ J Nat Sci. 2024;29(6):572–8.

[27] Wang F, Ali SN, Ahmad I, Ahmad H, Alam KM, Thounthong P. Solution of Burgers' equation appears in fluid mechanics by multistage optimal homotopy asymptotic method. Thermal Sci. 2022;26(1 Part B):815–21.

[28] Iqbal I, Boulaaras SM, Rehman HU, Saleem MS, Chou D. Navigating waves: Advancing ocean dynamics through the nonlinear Schrödinger equation. Nonlinear Eng. 2024;13(1):20240025.

[29] Rehman HU, Aljohani AF, Althobaiti A, Althobaiti S, Iqbal I. Diving into plasma physics: dynamical behaviour of nonlinear waves in (3+1)-D extended quantum Zakharov–Kuznetsov equation. Opt Quantum Electr. 2024;56(8):1336.

[30] Iqbal I, Rehman HU, Ashraf H, Walait A, Turki NB, Shah BH, et al. Soliton unveilings in optical fiber transmission: Examining soliton structures through the Sasa–Satsuma equation. Results Phys. 2024;60:107648.

[31] Zhu C, Idris SA, Abdalla MEM, Rezapour S, Shateyi S, Gunay B. Analytical study of nonlinear models using a modified Schrödingeras equation and logarithmic transformation. Results Phys. 2023;55:107183.

[32] Kai Y, Yin Z. Linear structure and soliton molecules of Sharma-Tasso-Olver-Burgers equation. Phys Lett A. 2022;452:128430.

[33] He Y, Kai Y. Wave structures, modulation instability analyzis and chaotic behaviours to Kudryashov's equation with third-order dispersion. Nonlinear Dyn. 2024;112(12):10355–71.

[34] Xie J, Xie Z, Xu H, Li Z, Shi W, Ren J, et al. Resonance and attraction domain analyzis of asymmetric duffing systems with fractional damping in two degrees of freedom. Chaos Solitons Fractals. 2024;187:115440.

[35] Kumar S, Kumar A, Wazwaz AM. New exact solitary wave solutions of the strain wave equation in microstructured solids via the generalized exponential rational function method. Europ Phys J Plus. 2020;135(11):1–17.
[36] Kumar A, Kumar S, Bohra N., Pillai G, Kapoor R, Rao J. Exploring soliton solutions and interesting wave-form patterns of the (1+1)-dimensional longitudinal wave equation in a magnetic-electro-elastic circular rod. Opt Quant Electron. 2024;56(6):1029.
[37] Kumar D, Saharan A, Kumar A. Exploring soliton patterns and dynamical analyzis of the solitary wave form solutions of the (3+1)-dimensional Wazwaz-Benjamin-Bona-Mahony equation. Modern Phys Lett B. 2025;39:2550102.
[38] Hussain E, Shah SAA, Bariq A, Li Z, Ahmad MR, Ragab AE, et al. Solitonic solutions and stability analyzis of Benjamin Bona Mahony Burger equation using two versatile techniques. Sci Rep. 2024;14(1):13520.
[39] Hussain E, Mutlib A, Li Z, E. Ragab A, Shah SA, Az-Zo'biEA , et al. examination of solitary waves for Sharma-Tasso-Olver Burger equation by stability and sensitivity analyzis. Zeitschrift für angewandte Mathematik und Physik. 2024;75(3):96.
[40] De Boor C, De Boor C. A practical guide to splines. Vol. 27. New York: Springer. 1978. p. 325.
[41] Raslan KR, El-Danaf TS, Ali KK Collocation method with quantic B-spline method for solving Hirota-Satsuma coupled KDV equation. Int J Appl Math Res. 2016;5(2):123–31.
[42] Liu F, Zhuang P, Turner I, Burrage K, Anh V. A new fractional finite volume method for solving the fractional diffusion equation. Appl Math Model. 2014;38(15–16):3871–8.
[43] Lin Y, Xu C. Finite difference/spectral approximations for the time-fractional diffusion equation. J Comput Phys. 2007;225(2):1533–52.
[44] Ghafoor U, Abbas M, Akram T, El-Shewy EK, Abdelrahman MA, Abdo NF An efficient cubic B-spline technique for solving the time fractional coupled viscous Burgers equation. Fract Fract. 2024;8(2):93.
[45] Abbas M, Majid AA, MdIsmail AI, Rashid A. Numerical method using cubic B-spline for a strongly coupled reaction–diffusion system. PLoS One. 2014;9(1):e83265.
[46] Rubin SG, Graves Jr RA. A cubic spline approximation for problems in fluid mechanics. No. L-9929. 1975.
[47] Akram T, Abbas M, Ali A, Iqbal A, Baleanu D. A numerical approach of a time fractional reaction–diffusion model with a non-singular kernel. Symmetry. 2020;12(10):1653.
[48] Akram T, Abbas M, Ali A. A numerical study on time fractional Fisher equation using an extended cubic B-spline approximation. J Math Comput Sci. 2021;22(1):85–96.
[49] Siddiqi SS, Arshed S. Quintic B-spline for the numerical solution of the good Boussinesq equation. J Egypt Math Soc. 2014;22(2):209–13.
[50] Iqbal MK, Abbas M, Nazir T, Ali N. Application of new quintic polynomial B-spline approximation for numerical investigation of Kuramoto-Sivashinsky equation. Adv Differ Equ. 2020;2020:1–21.